Vilniaus universiteto
Fizikos fakulteto
Lazerinių tyrimų centras

Naglis Kyžas

ALIUMINIO OKSINITRIDO PLONŲ SLUOKSNIŲ FORMAVIMAS IR JŲ TAIKYMAS OPTINĖSE DANGOSE

Magistrantūros studijų baigiamasis darbas

Lazerinės technologijos
studijų programa

Studentas	Naglis Kyžas
Leista ginti	2020-05-27
Darbo vadovas	dr. Alexandr Belosludtsev
Konsultantas	doc. dr. Andrius Melninkaitis
Centro direktorius	doc. dr. Aidas Matijošius

Vilnius 2020

TABLE OF CONTENTS

INTRODUCTION 3
1. LITERATURE OVERVIEW 4
  1.1 Magnetron sputtering 4
    1.1.1 Magnetron sputtering process 4
    1.1.2 Reactive magnetron sputtering 5
  1.2 Optical coatings 6
    1.2.1 Metal thin films based optical coatings 6
    1.2.2 Dielectric films based optical coatings 8
    1.2.3 Rugate coatings 10
  1.3 Metal oxynitride thin films 11
    1.3.1 Effective medium approximations 13
2. SUBSTRATES PREPARATION AND SAMPLES DEPOSITION 14
  2.1 Substrates preparation 14
  2.2 Samples deposition technique 14
3. SAMPLES INVESTIGATION TECHNIQUES 17
  3.1 Optical broadband monitoring (BBM) 17
  3.2 Spectrophotometer 17
  3.3 OptiLayer software pack 17
  3.4 Atomic force microscopy (AFM) 18
  3.5 Interferometer 19
  3.6 Transmission electron microscopy (TEM) 20
  3.7 Bandgap determination 21
4. RESULTS 22
  4.1 Discharge and deposition characteristics 22
  4.2 Aluminum oxynitride films properties 23
  4.3 Antireflective coatings design 26
  4.4 Antireflective coatings characterization 28
  4.5 Quasi - Rugate filter design 31
MAIN RESULTS AND CONCLUSIONS 34
REFERENCES 35
SUMMARY 41
SANTRAUKA 42

INTRODUCTION

These days there are bunch of applications for thin film coatings which are used in our everyday life. They are used for magnetic recording [1], electronic semiconductor devices [2], LEDs [3], hard coatings [4], energy generation [5] and storage [6]. Moreover, thin films are also used in optical components. Fabrication of antireflective [7], high reflection [8], polarizing [9] coatings and other optical components also relies on thin film techniques. As the laser industry is growing faster and faster every day, more optical components are needed.

Metallic oxynitride films are attracting researchers' because of their unique properties. They might be applied, for example, in protective coatings applications [10], gas barriers [11], optoelectronics [12], solar cells [13]. One of the most promising oxynitride property is the possibility to change optical, electrical, structural properties by varying oxygen-to-nitrogen ratio in the films. In works [14]–[19], investigations for TaN_xO_y, CrN_xO_y, ZnN_xO_y, NbN_xO_y, HfN_xO_y oxynitrides were done.

Aluminum oxynitride (AlN_xO_y) is one of attractive materials for investigation of tunable properties by changing oxygen and nitrogen content. This possibility arises from the particular characteristics of each base materials (Aluminum nitride - AlN and Aluminum oxide - Al_2O_3). AlN is a semiconductor material which refractive index varies from 1.8 and 2.2, bandgap is 5.8-6.2 eV. AlN is commonly used in preparation of optical sensors, light-emitting diodes [20]. In comparison, Al_2O_3 is an insulator, which refractive index is 1.7-1.8 in visible range. Al_2O_3 is often used as a protective layer for metal reflectors, dark mirrors and in metal-oxide-semiconductor devices [21]. The preparation of AlN_xO_y films may give a possibility to combine in it the properties of both AlN and Al_2O_3 materials. Oxynitride film properties may be tuned according to the required application. Afterwards, these oxynitrides might be used in more complicated multilayer coatings.

The aim of this work is to investigate possible applications of aluminum oxynitride thin films in optical coatings. In order to reach the aim, several tasks must be done: 1) investigate reactive magnetron sputtering process with metallic aluminum target and two reactive gases; 2) characterize deposited aluminum oxynitride films with various nitride fractions; 3) model and characterize multilayer antireflective coating using aluminum oxynitride layers; 4) model quasi – Rugate filter consisting of alternating fraction aluminum oxynitride films.

Main results of this work are summarized and published in high impacted journal *Optical Materials* [22]. Also part of the results were presented in international conference [23].

1. LITERATURE OVERVIEW

1.1 Magnetron sputtering

1.1.1 Magnetron sputtering process

Material sputtering is one of the process that occurs in material when it is under bombardment of high energy ions or neutral atoms. It is caused of the angular momentum exchange between bombarding and target material particles. Sputtering is activated when bombarding ions or atoms kinetic energy is higher than target material bond energy [24].

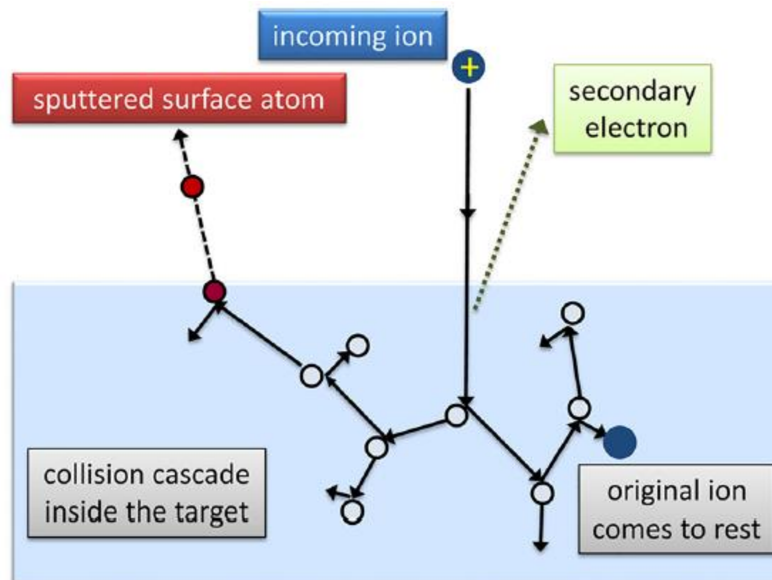

Fig. 1. Material sputtering process [25].

Magnetron sputtering technology relies on cross field (electric and magnetic) configuration, which lets to increase electron density above the cathode (which is sputtering material) and this leads to intensified density of plasma and greater speed of sputtering. This is because electrons are affected by electric and magnetic fields and because of Lorentz force they are moving in spiral trajectories, in this type of configuration. This way probability of ionization of inert gas (for example, Argon (Ar)) increases and as mentioned before – plasma intensifies [26].

Pulsed DC (p-DC) power supply configuration is widely used for metal oxides and other dielectric films deposition using metallic targets. During the negative part of the pulse, usual sputtering process is active: target is charged negatively, therefore positively charged Ar ions bombard it and material atoms with secondary electrons are being sputtered (Fig. 1). Neutral sputtered material atoms are deposited on the substrates. Secondary atoms ionize Ar gas atoms and the process is continued. During positive part of the pulse, electrons are moving towards target (because it is charged positively) and they neutralize positive charge which accumulated during the negative part of the

pulse. Usually negative part of the pulse is much longer than the positive pulse. This way, arcing caused by the accumulated positively charged layer on top of the target is avoided [27].

1.1.2 Reactive magnetron sputtering

Reactive magnetron sputtering allows to deposit dielectric layers using metallic target. This type of sputtering is achieved when reactive gas is added to the process gas. This way, sputtered material atoms chemically react with reactive gas which is injected into the vacuum chamber and forms chemical compound molecules which are deposited on the substrate. Moreover, when there is too much reactive gas in the vacuum chamber, reactive gas reacts with a metallic target and forms a layer of a nitride or oxide on top of it. Then target gets poisoned and the deposition speed drastically decreases [28], [29].

It is caused because chemical bond strengths of compounds are generally much stronger than the bonds of metal atoms so more energy is needed to break the bonds when the target is poisoned. This poisoning is highly undesirable. Moreover, there is a phenomena of hysteresis [30], [31] which is also redundant. Therefore, it is necessary to add just enough reactive gas to obtain a compound film on the substrate, but to be able to sputter away the thin compound layer on the surface of the target, thereby maintaining a metal surface on the target. This type of reactive sputtering is called sputtering in transition mode [25].

In Fig. 2, classic solution that is used by mostly of research groups and industry (constant oxygen flow) is shown. Constant oxygen flow control exhibits several disadvantages such as low deposition rate and refractive index inhomogeneity during repetitive film growth at varying fractions [32].

For reactive sputtering control in transition mode several techniques are known:

- Closed-loop reactive gas control. By controlling target voltage, plasma emission monitoring (PEM) spectral lines, pressure or current;
- Increasing vacuum pumping speed;
- Periodical metal film oxidation in a separate chamber [24];
- Varying target-to-substrate distance [33];
- Introducing a baffle between the substrate and the target [34];
- Pulsed reactive gas flow [35], [36].

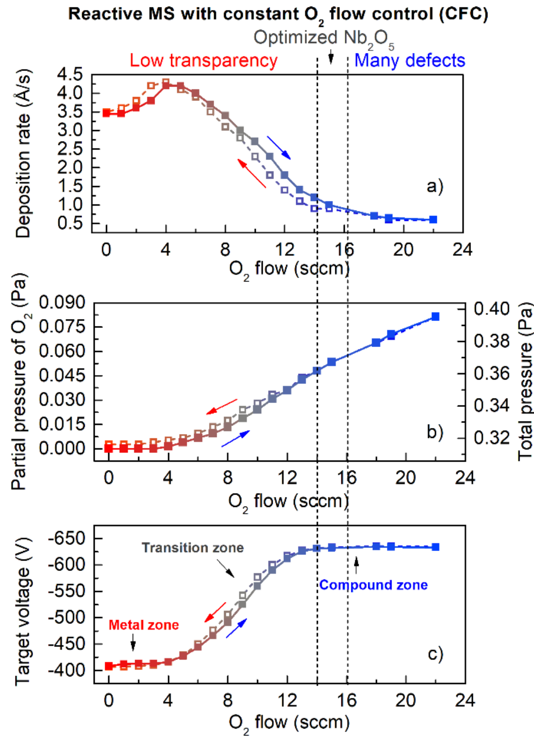

Fig. 2. Deposition rate (a), partial pressure of reactive gas (b) and target voltage (c) at various oxygen flow rates during reactive sputtering of metal niobium target with constant O_2 flow. Dash line marks experimentally determined optimal oxygen flow, which allows low absorption Nb_2O_5 films be deposited [32].

1.2 Optical coatings

Nowadays, optical coatings are widely used. Depending on the application, coating specifications may require specific transmittance and reflectance wavelength characteristics, polarization properties, group delay dispersion (GDD), laser-induced damage threshold (LIDT) values and other specifications. However, the majority desired characteristics of optical coatings are achieved by using two types of materials: thin metals and dielectric films.

1.2.1 Metal thin films based optical coatings

In general, metals can be described as a type of material having free carriers. When such a material is illuminated by electromagnetic radiation, electrons oscillate in response to an external electric field, but their oscillations are suppressed by collisions with other electrons, lattice ions, phonons, etc. These oscillations of electrons are described by *Drude* model [37]. According to *Drude* model, free electrons in matter induce the following electrical polarization **P**:

$$\boldsymbol{P}(\omega) = -\varepsilon_0 \frac{\omega_p}{(\omega^2 + \frac{i\omega}{\tau})} \boldsymbol{E} = -\varepsilon_0 \varepsilon_r \boldsymbol{E} \tag{1}$$

here ω_p- plasma frequency, ε_r- relative permittivity, ε_0- vacuum permittivity, amplitude of $\boldsymbol{E}$-oscillating electric field.

Plasma frequency may be described as:

$$\omega_p = \sqrt{\frac{Ne^2}{\varepsilon_0 m}} \tag{2}$$

here N- number density of electrons, e- electric charge, m- effective mass of the electron.

As it seen from the Eq. 1, relative permittivity which is described by *Drude* model is a complex quantity. Therefore, it is possible to separate real and imaginary parts:

$$\varepsilon_1(\omega) = 1 - \frac{\omega_p^2}{\omega^2+\gamma^2} \tag{3}$$

$$\varepsilon_2(\omega) = 1 - \frac{\omega_p^2}{\omega(\omega^2+\gamma^2)} \tag{4}$$

here γ- damping coefficient.

From the imaginary part of relative permittivity Eq. 4 it is seen that when $\omega > \omega_p$, imaginary part is insignificant and electron plasma as well as metal becomes transparent. This is due the inertia of the electrons in oscillation, electrons can no longer react to electric fields with a high oscillation frequency (high-frequency electromagnetic radiation), and as a result, metal become less and less absorbent as the wavelength decreases.

When $\omega < \omega_p$, electron plasma is absorbing incident electromagnetic radiation and it attenuates as it propagates. However, electromagnetic waves in plasma take the form of decaying standing waves, rather than travelling ones, so it does not propagate through the plasma, alternatively it is totally reflected.

Latter property of metals makes a thin metal layer deposited on the optical substrate the simplest optical coating which can work as a mirror. For example, aluminum thin film reflects 88% - 92% of incident light and can work in visible light range (Fig. 3). More expensive metals, such as silver or gold reflects up to 99% of incident light in visible or near infrared range. The downside of such type of coatings is that their reflectivity is in wide optical range and sometimes it is an undesirable characteristic of a mirror.

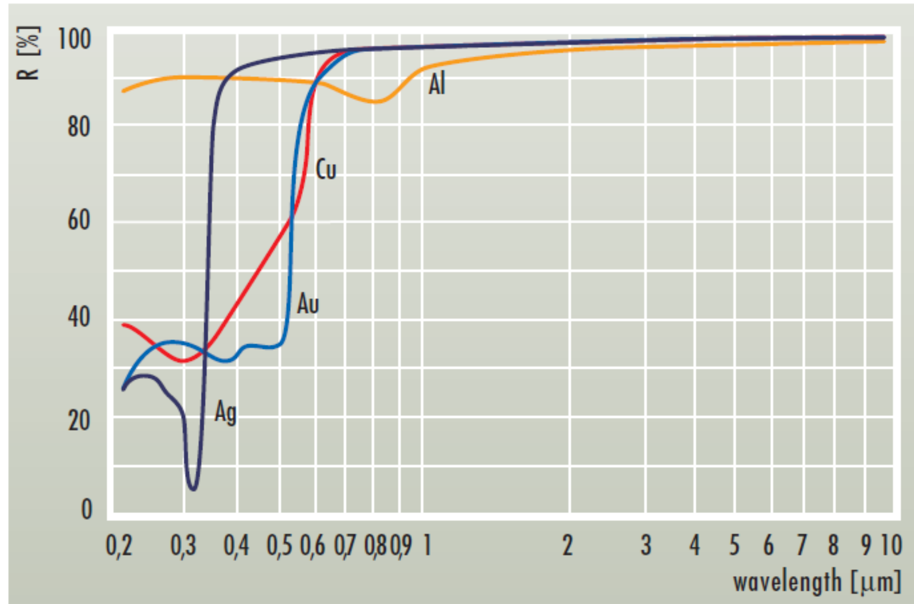

Fig. 3. Reflectivity of different metals [38].

1.2.2 Dielectric films based optical coatings

Interaction between dielectric materials and incident light traditionally is described by Lorentz oscillator model [39]. Lorentz proposed that the electron is bound to the nucleus of the atom by some force which behaves according to spring-like force. According to the Newton's second law this type of system may be described:

$$m\frac{d^2x}{dt^2} = \boldsymbol{F}_{driving} + \boldsymbol{F}_{damping} + \boldsymbol{F}_{spring} = -eE(t) - m\gamma\frac{dx}{dt} - m\omega_0 x \tag{5}$$

$F_{driving}$ is a force generated by electromagnetic wave illuminating a material (electric field of the electromagnetic wave forces the electron to move from a state of rest), $F_{damping}$ is a force generated due to collisions in lattice, electron radiation as it moves with acceleration, etc., F_{spring} is a force between nucleus of the atom and its electron.

Using Eq. 5 it is possible to derive polarization for dielectric material:

$$\boldsymbol{P}(\omega) = \frac{\varepsilon_0\omega_p^2}{(\omega_0^2-\omega^2)+i\gamma\omega}\boldsymbol{E} \tag{6}$$

Therefore, complex relative dielectric permittivity is described as:

$$\varepsilon_r = \frac{\varepsilon}{\varepsilon_0} = \frac{\omega_p^2}{(\omega_0^2-\omega^2)+i\gamma\omega} + 1 \tag{7}$$

From Eq. 7, real and imaginary parts of relative dielectric permittivity can be separated:

$$\varepsilon_1(\omega) = 1 + \chi + \frac{\omega_p^2(\omega_0-\omega)}{(\omega_0^2-\omega^2)^2+(\omega\gamma)^2} \tag{8}$$

here χ is dielectric susceptibility.

$$\varepsilon_2(\omega) = 1 - \frac{\omega_p^2 \omega\gamma}{(\omega_0^2 - \omega^2)^2 + (\omega\gamma)^2} \quad (9)$$

When frequency of incident electromagnetic wave is far away from the resonant frequency, imaginary part of relative dielectric permittivity is negligible, therefore absorption of dielectric material is very low for given frequency. It means that dielectric materials are transparent in wide range of frequencies between infrared resonant frequency of the vibrational energy levels of the molecules and ultraviolet resonant frequency of the electron energy levels. This property makes them suitable for interference optical coatings applications in the range from ultraviolet up until infrared range.

Dielectric films based optical coatings usually are formed using oxide layers or in some occasions using metal nitrides or fluorides (e. g. SiO_2, Nb_2O_5, MgF_2, AlN, etc.). Material of choice depends on their refractive indices and extinction coefficients in specific spectral range depending on the desired application. By varying materials with different refractive indices, their thicknesses and layers number mirror (reflectivity >99,99%), antireflective (reflectivity <0,1%), beam splitting or filter coatings for specific wavelength may be prepared. Because of number of applications dielectric coatings are used in many devices, such as lasers, microprocessors, interferometers [40].

Dielectric coatings usually consist of two dielectric materials: high and low refractive index. They are being formed on optical substrates in alternating layer structures. Incident light is being partly reflected from each interface and all reflected waves interfere with each other. Type of the interference is determined by the phase difference between these reflected waves. If they are in-phase, constructive interference is formed and it results in enhanced resulting wave, if they are opposite phase – it is destructive one which leads to reflected wave elimination (Fig. 4) [41].

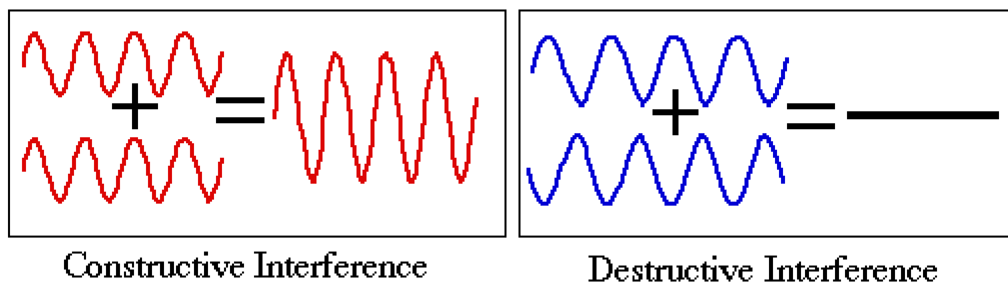

Fig. 4. Schematic picture of constructive and destructive interference.

For manufacturing multilayer dielectric mirror coatings constructive interference is used. Conventionally, optical thickness of every layer is formed to be quarter of the incident light wavelength ($\lambda_0/4$). Coherent waves reflected from each interface between separate layers interfere with each other and new superposed wave appears. It happens because reflected rays from different

high – index layers and low – index layers are in-phase and their path length difference (*PLD*) is satisfying condition of interference maximum:

$$\Delta PLD = n\lambda \tag{10}$$

here n = 0; 1; 2; 3…; λ – wavelength of incidence light.

Antireflective coatings physical principle is similar to dielectric mirrors just they are based on destructive interference. Condition of destructive interference for *PLD*:

$$\Delta PLD = \left[n + \frac{1}{2}\right]\lambda \tag{11}$$

here n = 0; 1; 2; 3…; λ – wavelength of incidence light.

Structure of such coatings contains only several layers. Thickness of these layers are selected such that reflected waves from every interface would be in opposite phase, therefore these rays eliminate each other.

1.2.3 Rugate coatings

There are several drawbacks of using conventional high and low refractive structure dielectric for building the interference coatings. One of the solutions to extend the possibilities and properties of such coatings is to build Rugate type of coatings. The Rugate type of coatings are optical coatings which have evenly oscillating refractive index (gradient-index) throughout the coating (Fig. 5) [42]. As well as quarter wavelength high and low refractive index material stacks, this periodically oscillating refractive index distribution is forming low transmittance zone, but in this case it is π/4 narrower than in classical solution. Optical properties of this type of coating are described by four parameters: average refractive index N_0, amplitude of refractive index modulation ΔN, period of the modulation P and number of periods n. P determines the wavelength of the reflection zone, ΔN defines the width of the reflection zone, n decides the level of the maximum reflection and N_0 specifies coating thickness and its sensitivity to the incident angle (higher N_0 influences lower angular sensitivity).

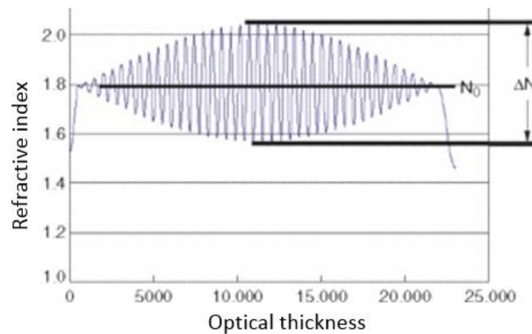

Fig. 5. Typical refractive index profile for a Rugate coating.

External media of the coating are substrate and air which refractive indices do not match with the first and last layers of Rugate coatings in most cases. Due to multiple reflections between coating - air and coating - substrate interfaces, interference fringes are observed in spectra. In order to reduce this effect, index – matching layers which coincide the refractive indices between the coating and air/substrate are introduced into design. Index – matching layers consist of certain number of layers with specific refractive index distribution until its refractive index matches mean refractive index of Rugate coating, N_0 [43]. Moreover, this type of optical coating design enables opportunity to eliminate higher harmonics (Fig. 6) [44].

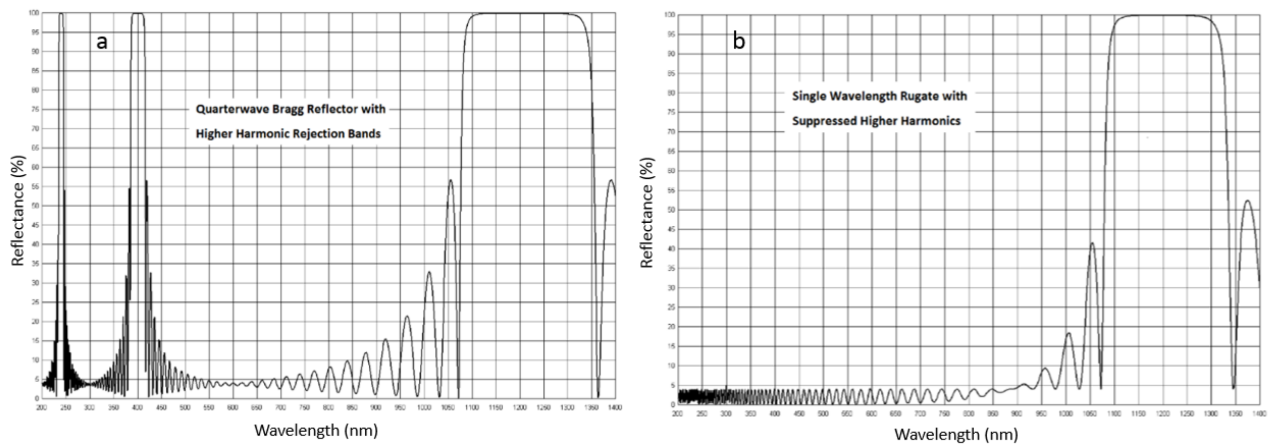

Fig. 6. Spectral characteristics of quarter-wave (a) and Rugate (b) coatings [45].

However, modelling and manufacturing of these coatings is a technological challenge. It requires high precision process parameters adjustment; it is highly time consuming and materials should be precisely characterized both optically and physically.

Coatings with alternating refractive index distribution enables formation of antireflective coatings [46], short-pass, band-pass and spectral filters [42]. Although, it is also possible to design such coatings using only two different refractive index materials, Rugate structures remain the only ones which forms high optical transmittance bands in wide spectral range.

1.3 Metal oxynitride thin films

One of the possible type of materials for alternating refractive index Rugate coatings formation are metal oxynitride films. Optical properties of these materials, together with their excellent mechanical strength, thermal properties and chemical stability allows them be used for optical coatings applications. Moreover, optical properties of the films are strongly related to the electronic band structure and can be varied significantly by changing the chemical composition which might be carried out by varying oxygen and nitrogen content in the films. It enables an opportunity to vary refractive index, extinction coefficient and band gap of the deposited film [47].

S. Venkataraj et al. [18] showed that increase of nitrogen fraction in metal oxynitride film, increased both the index of refraction as well as the extinction coefficient of the films. Likewise, increasing nitrogen fraction in oxynitride films leads to reduced band gap of the film (Fig. 7). This can be explained considering the fact that the N 2*p* orbitals have higher potential energy than O 2*p*, therefore nitrogen atoms incorporation into oxygen sublattice leads decreased band gap [47].

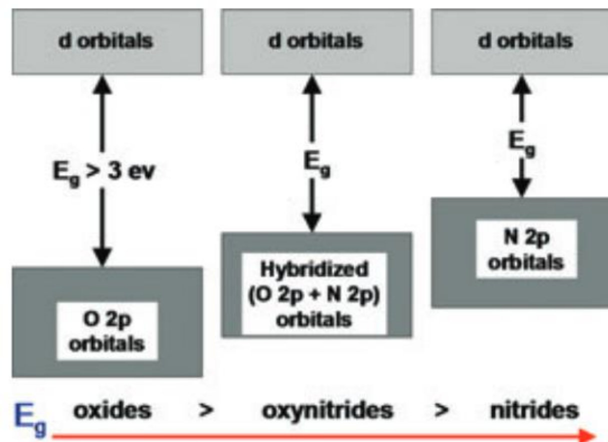

Fig. 7. Schematics of band structures of oxides, oxynitrides and nitrides [47].

Silicon oxynitride (SiON) is one of the most commonly used oxynitride materials in optical coatings applications. It attracts great interest not only because of its excellent properties such as chemical inertness, high thermal stability and corrosion resistance, but also because of its combination of adequate mechanical, optical and electrical properties. It was reported [48] that it is possible to tune refractive index of silicon oxynitride in the wide range between 1.45 (λ = 550 nm for silicon oxide) to 2.05 (λ = 550 nm for silicon nitride) using reactive radio frequency sputtering from Si target. Silicon oxynitride films were used for production of antireflective coatings, Rugate filters, edge filters, dichroic filters production [49].

S. H. Mohamed et al. [20] showed that by varying nitrogen content in the reactive gas during reactive magnetron sputtering of titanium target is possible to increase refractive index, film density and deposition rate of titanium oxynitride films by 15%. Although, higher fraction of nitrogen reduces optical bandgap from 3.29 eV (TiO_2) to 2.11 eV (TiN) it is said that TiON is a promising functional optical material in the visible range.

Zirconium oxynitride films are high refractive index materials with a tunable refractive index from 2.11 to 2.26 at 650 nm. Moreover, it was shown that it is possible to increase deposition rate by more than a factor of 3 while increasing nitrogen partial pressure at the same time reducing roughness of the films [50]. Nevertheless, band gap of the films decreases, but they remain transparent in visible range which makes them applicable in optical coatings.

1.3.1 Effective medium approximations

Deposited composite films might be treated as two separate consisting materials (in the case of AlO_xN_y, it may be separated into Al_2O_3+AlN) for their characterization. Therefore, relationship between optical properties of and composition of composite is described by effective medium approximations (EMA). Using effective medium approximations effective dielectric constant is described using dielectric constants and volumetric concentrations of consisting materials.

Maxwell-Garnett, *Bruggeman* and *Lorentz-Lorenz* models are the most used ones for effective medium approximations. The first two depends on calculations of different phase for each consisting materials in a compound. *Maxwell-Garnett* model says that particles of the second material are spread in the first material [51], while *Bruggeman* model states that particles of different materials are randomly mixed with each other [52]. *Lorentz-Lorenz* model relies on averaging polarization of molecules of the compounds, therefore differences of phases are not determined there [53].

Dielectric constant ε consists of real and imaginary parts (ε' ir ε''). Relathionsips between them and refractive index and extinction coefficient are:

$$\varepsilon' = n^2 - \kappa^2 \tag{12}$$

$$\varepsilon'' = 2n\kappa \tag{13}$$

here n – refractive index, κ – extinction coefficient.

Extinction coefficient κ can be eliminated if calculations are in spectral range where absorption is non-existent or negligible then $\varepsilon''= 0$.

Formulas describing *Maxwell-Garnett*, *Bruggeman* and *Lorentz-Lorenz* approximation models:

$$\textit{Maxwell-Garnett:}\ \frac{\varepsilon_{eff}-\varepsilon_H}{\varepsilon_{eff}+2\varepsilon_H} = (1-f_H)\frac{\varepsilon_L-\varepsilon_H}{\varepsilon_L+2\varepsilon_H} \tag{14}$$

$$\textit{Bruggeman:}\ f_H\frac{\varepsilon_H-\varepsilon_{eff}}{\varepsilon_H+2\varepsilon_{eff}} + (1-f_H)\frac{\varepsilon_L-\varepsilon_{eff}}{\varepsilon_L+2\varepsilon_{eff}} = 0 \tag{15}$$

$$\textit{Lorentz-Lorenz:}\ \frac{\varepsilon_{eff}-1}{\varepsilon_{eff}+2} = f_H\frac{\varepsilon_H-1}{\varepsilon_H+2} + (1-f_H)\frac{\varepsilon_L-1}{\varepsilon_L+2} \tag{16}$$

here f_H – volumetric fraction of high index material. Indices *eff, H, L* denote effective, high refractive index and low refractive index medium respectively.

2. SUBSTRATES PREPARATION AND SAMPLES DEPOSITION

It is essentially important to select proper substrates cleaning and samples preparation techniques. Effectivity of coating characteristics highly depend on substrate quality and deposition conditions. Even small pieces of dust might dramatically change coating properties, therefore it is very important to look after samples before, during and after deposition process.

2.1 Substrates preparation

All of the depositions were made on double-sided polished fused silica (FS) substrates. Before the depositions, they all were cleaned using ultrasonic cleaning machine (Optimal "40MF Mk2") in order to remove dusts and dirt which is on the surface of the substrates.

Ultrasonic cleaning process consists of 4 baths. First bath is filled with potassium hydroxide (KOH) solution and ultrasonic is applied here. During the process in the first bath ultrasonic creates vibrations and bubbles inside the solution which remove dusts and dirt from the surface of the substrates [54]. Ultrasonic in the pure water is applied in the second bath. The process works in the similar way as in the first bath. Then the process comes to the third bath which is filled with deionized water in order to clean all the remaining dusts and remove KOH solution from the substrates. In the final bath, the substrates are heated in the 50-60°C temperature in order to dry them off and not to leave any stains on the substrates. The lengths of the processes in each bath are 350s, 400s, 300s, 350s, respectively.

2.2 Samples deposition technique

All the samples are prepared using Kurt J. Lesker Company (PVD225) magnetron sputtering system (Fig. 8).

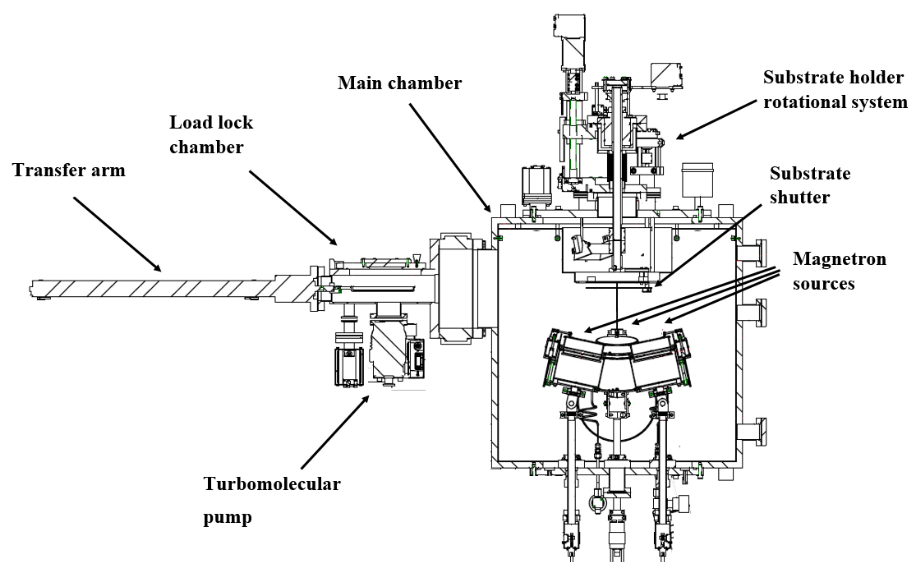

Fig. 8. Schematic drawing of Kurt J. Lesker magnetron sputtering system PVD225.

It consists of two interconnected chambers: load lock and main chamber. For pumping down the vacuum in the load lock, scroll pump (XDS 35i from Edwards; 11 L/s air) and turbomolecular (HiPace 80 from Pfeiffer Vacuum; 67L/s air) pumps are used. Main chamber is equipped with the same scroll pump and cryogenic pump (Cryo-Torr 8F series from Helix Technology Corporation; 1500L/s for air).

Firstly, cleaned substrates are inserted into load lock chamber and the chamber is pumped to pressure of 10^{-2} Torr using scroll pump. After turbomolecular pump is started and pressure in load lock has reached 5×10^{-6} Torr substrates are loaded into the main chamber. Before this, main chamber should be pumped down to the base pressure of 5×10^{-7} Torr using cryogenic pump.

There are two types of pressure gauges in the main chamber. One of them is capacitance manometer which measures pressure up to 1 mTorr and it is used to measure pressure during the deposition process. The other one is ion gauge; it measures vacuum above that value and is used for base pressure estimation.

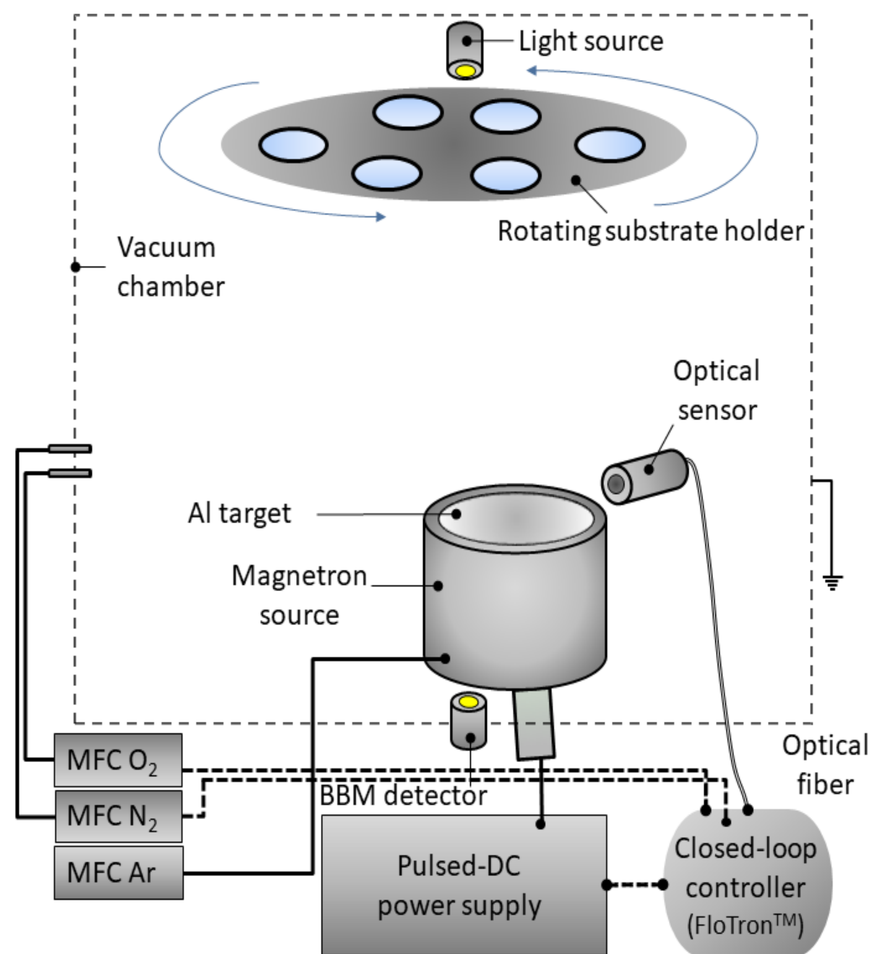

Fig. 9. Schematic diagram of the deposition setup with one magnetron source and two reactive gases connected.

In the main chamber of sputtering system, there are unbalanced magnetron sources (Torus™ sputter guns) with planar targets mounted on top of them (Fig. 9). The magnetron sources are driven by a pulsed DC (p-DC) power supply (Advanced Energy Pinnacle Plus). All process gases used for depositions are >99.999 % pure. The Ar flow rate is 20 sccm and the pumping speed is adjusted to attain the Ar pressure at the same value of 2.2 mTorr. The settings of the Ar flow rate and the pumping speed are not changed during the processes. Prior every deposition, the target is pre-sputtered for 5 min in Ar to remove any surface oxides.

During all depositions substrate holder is constantly rotating (20 rounds per minute) in order to reach better uniformity of deposited layer [55] and to monitor layer thickness by Optical Broadband Monitoring (BBM).

For oxide films deposition in reactive mode it is needed to control oxygen injection into the chamber. In this case, it is done using closed-loop controller Flotron™ X3 (Nova Fabrica). This device lets to use one out of two modes of operation:

- Direct mode. In this mode of operation oxygen flow is controlled directly and is not affected by any process control algorithms.
- Feedback mode. Oxygen flow in this mode of operation is calculated by a Pseudo-derivative-feedback (PDF) control algorithm based on defined sensor value and its deviation from a user defined set-point. The PDF control algorithm is described more in details in Ref. [56].

3. SAMPLES INVESTIGATION TECHNIQUES

For samples characterization *in-situ* during the deposition process, magnetron sputtering system is equipped with:

3.1 Optical broadband monitoring (BBM)

BBM system is used to measure transmittance spectrum of the samples during the deposition process and to calculate thickness of thin film layer. It consists of light source which is located above the substrates holder (Fig. 9), detector connected to spectrophotometer with a high-speed CCD camera and BBM software.

Recording and data acquisition of spectra can be performed for preselected positions on a fixed radius of the substrate holder, so before a deposition process BBM system needs to be calibrated. For this purpose, a 100% spectrum of an empty position and a spectrum of an area with zero transmittance are measured and taken as the normalization basis for the sample spectra.

CCD camera, which is used in the magnetron sputtering system, is sensitive in a wavelength range from 400 to 1000 nm. BBM software is used to calculate layer thickness from the measured transmittance spectrum of a sample. It fits measured spectra with a theoretical one until it reaches the minimum value of mean squared error (MSE) [57].

After deposition, processed samples are removed from the vacuum chamber and further investigated using several coatings characterization techniques:

3.2 Spectrophotometer

For transmittance, *T* and reflectance, *R* spectra were measured with the angle of incidence (in reflection) 8° in the $185<\lambda<1300$ nm wavelength range using a Photon RT (Essent Optics) spectrophotometer. It consists of light source, monochromator, which is diffraction grating and detector. Light emitted from the broadband light source is being filtered and different wavelengths of light are directed towards the sample. Transmitted and reflected light intensities measured by detector are compared with base transmittance value of the specific wavelength. This way transmittance and reflectance values of the sample can be calculated. For measuring different polarizations of the light, polarizers are included in the measuring unit.

3.3 OptiLayer software pack

Optical constants (refractive index, *n* and extinction coefficient, *k*) of films for every layer were determined from transmittance and reflectance spectra, using the "OptiChar v8.85" software from

OptiLayer Ltd. [58]. This software incorporates a lot of different models for $n(\lambda)$ and $k(\lambda)$ determination, however the following ones have been used specifically in this work:

$$n(\lambda) = n + \frac{A}{\lambda^2} + \frac{B}{\lambda^4} \tag{17}$$

$$k(\lambda) = B_0 \exp\left(\frac{-B_1}{\lambda} - \frac{-B_2}{\lambda}\right) \tag{18}$$

Transmittance - reflectance spectra are fitted by adjusting A, B coefficients and physical thickness of the film until the discrepancy between theoretical and the measured spectrum were minimized.

“OptiChar” software also includes Bruggeman effective medium approximation model (see Sec. 1.3.1) which enables the possibility to model volumetric concentrations of deposited film.

Multilayer structures were modelled using “Optilayer v8.84” software. When starting coating structure is unknown, random optimization tool is used to carry out a sequence of optimization procedures with random starting designs. This step helps to find a starting design with better manufacturability. After that, selected design is being optimized by one of the chosen numerical methods. It is done by optimizing the merit function with respect to the layer thickness. Merit function estimates the closeness between target and current spectral characteristics. In the simplest case when target reflectance on the wavelength grid $\{\lambda_j\}$, it is specified:

$$MF = \left[\frac{1}{L}\sum_{j=1}^{L}\left(\frac{R(X,\lambda_j)-\hat{R}(\lambda_j)}{\Delta R_j}\right)^2\right]^{1/2} \tag{19}$$

This step is called refinement of the design. Number of most powerful first, second and higher order routines can be used in this step: Hyper Newton method, Modified damped least squares, Newton’s 2nd order method, Quasi-Newton DLS, Sequential Quadratic Programming, Conjugate gradient and Steepest descent methods. User always can decide if merit function value is acceptable, target design is reached and modelling is completed [59].

3.4 Atomic force microscopy (AFM)

Surface roughness measurements were done using Dimension Edge atomic force microscope system by Veeco. AFM system consists of a micro-machined cantilever probe and a sharp tip mounted to Piezoelectric (PZT) actuator and a position sensitive photo detector for receiving a laser beam reflected off the end-point of the beam to provide cantilever deflection feedback. In tapping mode (T-AFM), the cantilever is oscillated at or near its natural resonant frequency using a PZT actuator and is moved across the measuring surface. When the tip passes over a bump in the surface, its vibration amplitude decreases due to availability of less vibrating space. When it passes over a depression, its vibration amplitude increases (approaching its free air amplitude). This change in oscillation

amplitude is detected by optical system and fed back to the controller which compares the measured value with the set reference value and generates an error signal. That error signal is a measure of the surface irregularities in the vertical position, so it can be used to plot the surface topography of the sample [60].

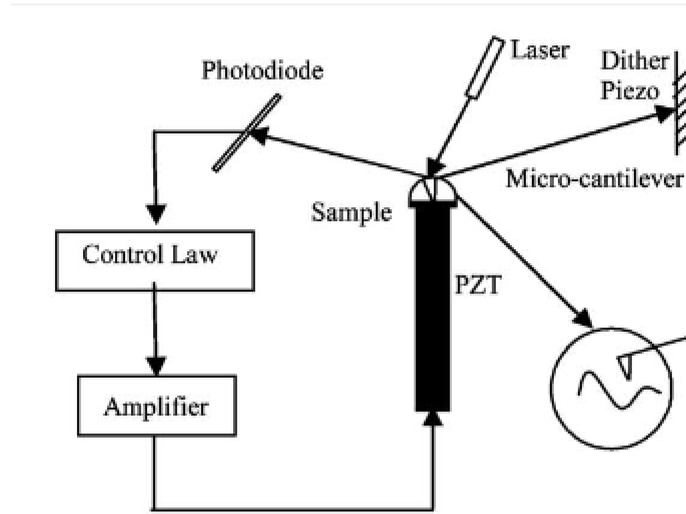

Fig. 10. Schematic of AFM operation [60].

Surface roughness was evaluated using root mean square (RMS) value which is calculated by the expression:

$$RMS = \sqrt{\frac{1}{N}\sum_{i=1}^{N}(Z_i - Z_{avg})^2} \quad (20)$$

here Z_i – height of i-th measurement, Z_{avg}- average height, N- number of measurements. Roughness measurements were taken in several separate areas (20 µm x 20 µm) of the sample.

3.5 Interferometer

In order to determine stress of the coatings, flatness of the samples should be measured. Fizeau interferometry method for flatness measurements was used (Fig. 11). Flatness measurements were done using interferometer MarSurf FI 1040 Z (Mahr GmbH). The aperture of 24 mm was used for measurements. The interferometric fringes were analyzed by the IntelliWave software.

Principle of the Fizeau interferometer: light (λ = 632.8 nm) from the source is condensed. Then the light passes through a pinhole and collimating lens projects a parallel beam of light onto the face of the gauge to be tested via an optical flat. This results in formation of interference fringes which are reflected back using a glass plate reflector. From the data of interference fringes, flatness of the workpiece is determined.

To estimate stresses of the coatings, Stoney method [61] was used. After measuring the samples with an interferometer, the flatness measurement data was used to calculate the stress of the film:

$$\sigma = \frac{E_s}{6(1-\nu_s)} \frac{t_s^2}{t_l} \left(\frac{1}{R_1} - \frac{1}{R_0}\right) \quad (21)$$

here E_s and ν_s are Young's modulus and Poisson ratio of the substrate, respectively, t_s and t_l are thickness of the substrate and layer, respectively, R_1 and R_0 are curvature radiuses of coated and uncoated substrate respectively.

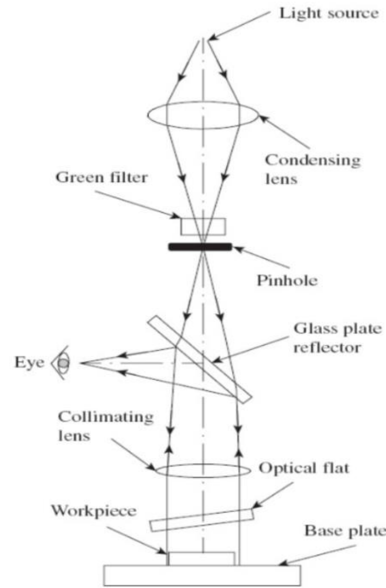

Fig. 11. Schematic view of interferometer for flatness measurements [62].

3.6 Transmission electron microscopy (TEM)

Cross-section picture of the coating was taken using transmission electron microscope FEI Tecnai G2 F20 X-TWIN TEM. During measurements it was operating at 200 kV voltage. Pictures were recorded using Orius CCD camera (Gatan). The sample was prepared by Ga ion milling on dual beam system FEI Helios Nanolab 650 equipped with an Omniprobe manipulator was used to prepare the cross-sectional TEM specimens. The sample was covered by the platinum layer.

This device illuminates the sample with a parallel electron beam and magnifies formed image on a phosphor screen (Fig. 12). Electron beam exiting the electron gun is collimated by a condenser lens and illuminates the sample. Electrons passing through the sample form an image that is magnified by two lenses and projected on fluorescent screen. The fluorescent image can be captured with a CCD camera or on a photographic film.

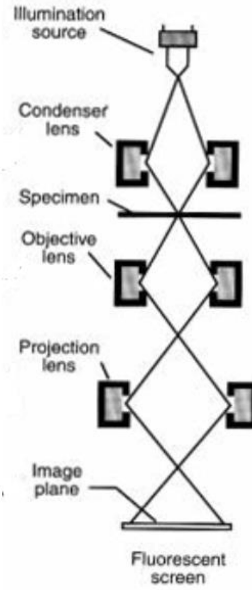

Fig. 12. Schematic picture of TEM [63].

3.7 Bandgap determination

The direct band gap (E_g) of the thin films was determined according to Tauc law [64]:

$$(\alpha h\nu)^2 = A(h\nu - E_g) \tag{22}$$

here $h\nu$ – photon energy, A – constant. Absorption coefficient (α) was determined from the optical transmittance and reflectance based on the expression:

$$\alpha = 2.303\frac{Abs}{d} \tag{23}$$

here d is physical film thickness, Abs is absorbance of the film. If scattering from the film is negligible, absorbance of the film may be calculated by the following equation:

$$Abs = 1 - R - T \tag{24}$$

here R and T are reflectance and transmittance values of the deposited film, respectively. Approximating the linear part of the dependence of $(\alpha h\nu)^2$ on $h\nu$, the point where abscissa axis ($h\nu$) is intersected corresponds to the numeric value band gap.

4. RESULTS

4.1 Discharge and deposition characteristics

In this part, investigation of reactive sputtering modes while changing reactive gases composition (oxygen and/or nitrogen) was done. Every deposition system has its special design and geometry, therefore it is essential to investigate sputtering conditions. Constant power mode of the power supply was used and the voltage changes on aluminum target were investigated.

When reactive gas is introduced into chamber, it reacts with sputtered aluminum atoms. Also the gas reacts with the sputtering target surface and may form compound layer on it. While decreasing the reactive gas flow, the compound layer on the surface of the target is being removed [28]. This way highly undesirable phenomena of hysteresis appears. With the lack of reactive gas or gases (metallic mode) under stoichiometric films with low transparency are done [65]. Aluminum oxynitride films deposited in metallic mode exhibit high extinction coefficient values. Oppositely, while the process is operating in excess amount of oxygen (poisoned mode), deposited films contain large amount of defects, deposition rate is very low and there are big instabilities in process.

The results of varying the reactive gas composition on power supply voltage are shown in Fig. 13. Nitrogen and oxygen gases flows were injected simultaneously during the experiment in order to reach the oxygen to nitrogen ratio as described in the graph. As it can be seen, with the increase of nitrogen content in reactive gas, the moment of target poisoning is shifting to the higher flow values. Similar behavior was observed in Ref. [66]. This phenomenon might be explained by aluminum higher affinity to oxygen than to nitrogen. The standard molar enthalpies of formation are − 1675.7 kJ/mol for Al_2O_3 [67] and − 318.0 kJ/mol for AlN [67]. Moreover, it can be seen that increased nitrogen ratio in reactive gases flow causes narrowed curve of hysteresis, which was also shown in Ref. [68].

To sum up, for high-rate stable process optimal reactive gases flows were found. Moreover, at such conditions optically transparent and defect-free films are deposited.

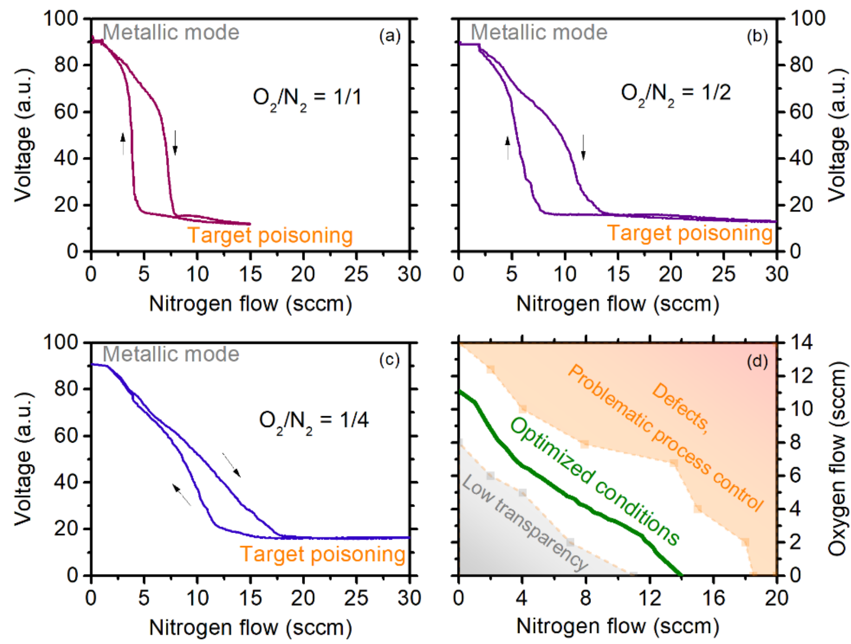

Fig. 13. Hysteresis loops of target voltage for various gas mixture with oxygen to nitrogen flow ratios a) 1:1, b) 1:2 and c) 1:4. Summary d) of approximate optimized conditions for oxynitrides deposition.

4.2 Aluminum oxynitride films properties

In this part, aluminum oxynitride films with various nitrogen fraction in the films are prepared and their optical properties and surface roughness are investigated.

Using optimized conditions determined in Sec. 4.1 6 aluminum oxynitride samples with various nitrogen fraction (0 %; 15 %; 37 %; 45 %; 70 % and 100 %) in the films were prepared. Their transmittance and reflectance spectra were measured. Results are shown in Fig. 14.

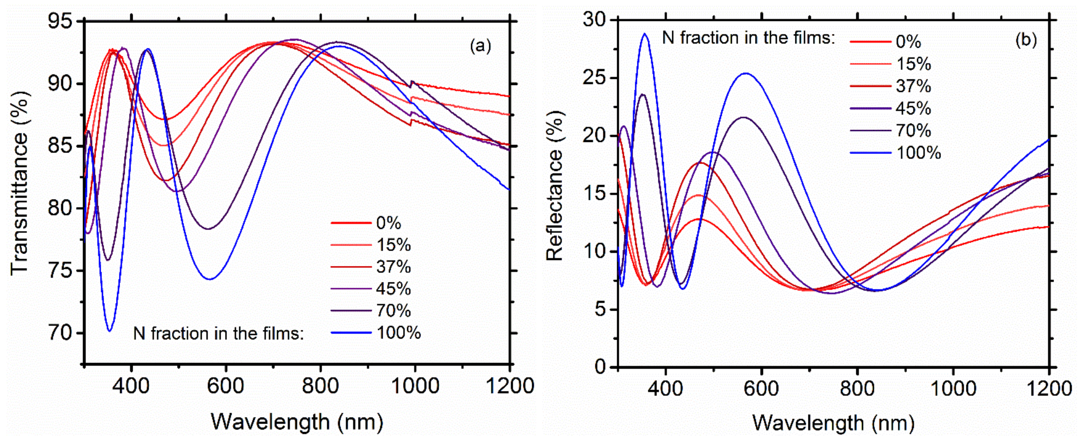

Fig. 14. Transmittance (a) and reflectance (a) spectra of aluminum oxynitrides prepared with various nitrogen fraction in the films.

The dispersions of the refractive index, *n*, and extinction coefficient, *k*, derived from analysis of the transmittance and reflectance spectra of various aluminum oxynitride films are introduced in Fig. 15. Refractive indices are increasing with the increase of nitrogen fraction in the films (Fig. 15a). Volumetric fractions of nitrogen in the films were determined by Bruggeman model (Sec. 1.3.1).

Similar increase of refractive index with the increase of nitrogen content in oxynitrides was reported before [69], [70]. Values of extinction coefficient have not significantly increased with nitrogen content (Fig. 15b), for all films they stayed at $k_{532} < 1x10^{-4}$. This way, by varying oxygen and nitrogen flows as reactive gases during magnetron sputtering process it is possible to tune refractive index of deposited thin film from $n_{532}(Al_2O_3)=1.67$ to $n_{532}(AlN)=2.1$.

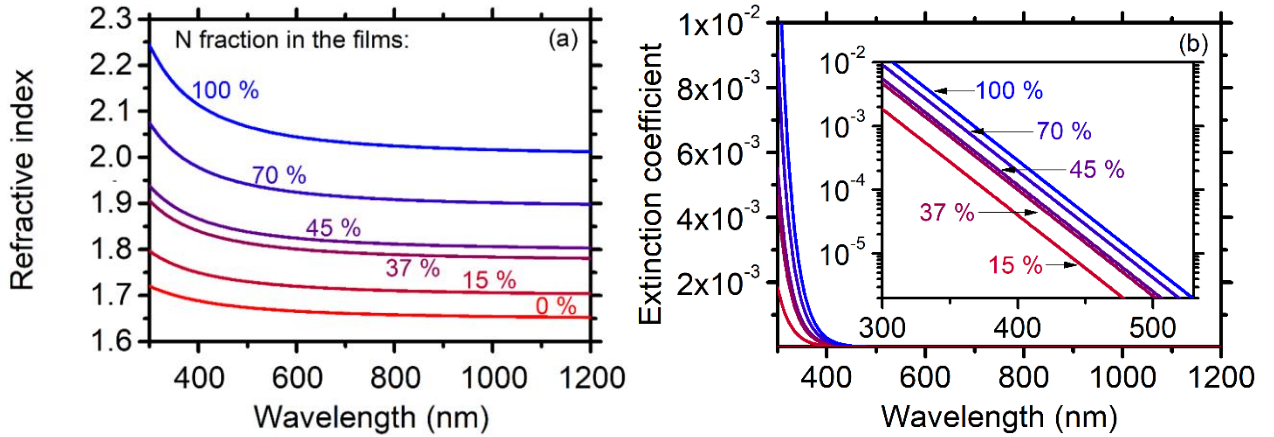

Fig. 15. Refractive index (a) and extinction coefficient (b) of aluminum oxynitrides prepared with various nitrogen fraction in the films.

Tauc plots which are used for direct optical band gap determination of the films are presented in Fig. 16.

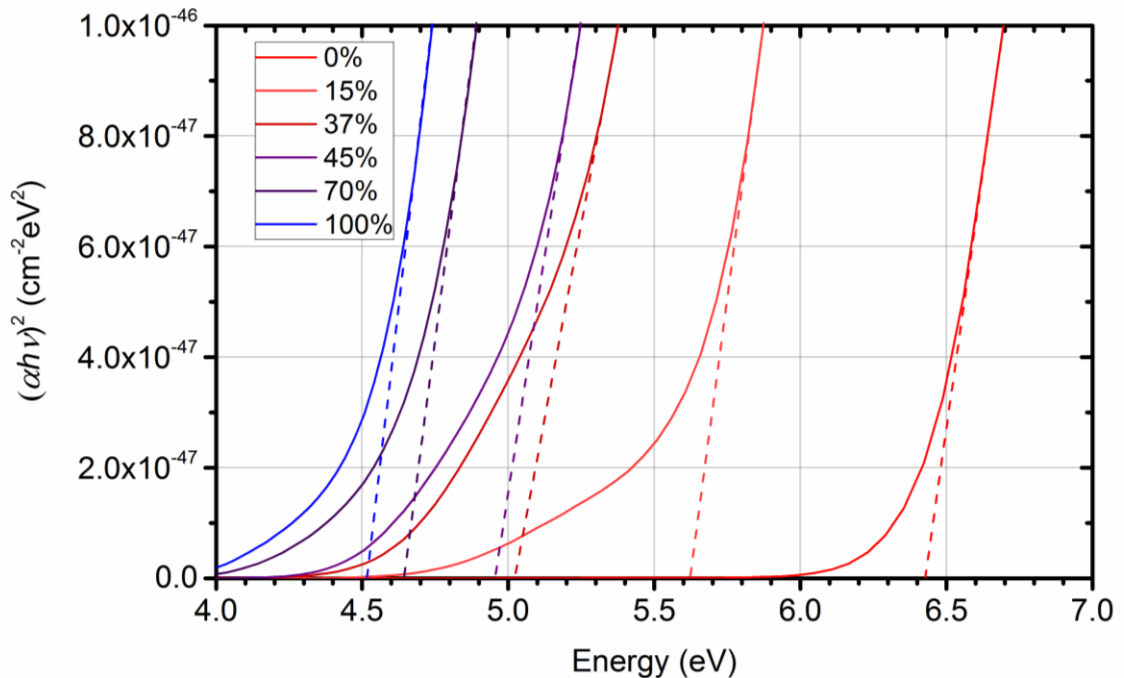

Fig. 16. Tauc plots of aluminum oxynitride films for optical band gap determination.

The highest band gap value is observed for Al_2O_3 is 6.42 eV, which falls in the range of values presented in published works (5.75 eV – 7 eV) [71], [72]. Whereas, AlN film demonstrates the lowest band gap – 4.51 eV. This value is corresponding to the reported value (4.5 eV) [73]. The band gap values of the remaining aluminum oxynitride films fall in the range between 4.64 eV to 5.62 eV

depending on the nitrogen fraction. Oxynitride films exhibit inverse correlation between AlN fraction in the film and the band gap of the film.

Surface roughness is one of the critical coating characteristics which needs to be maintained as low as possible for high quality optical components. Increased surface roughness might cause undesired scattering losses. In order to evaluate roughness of the deposited aluminum oxynitride films, AFM measurements were performed. The films topographies are shown in Fig. 17. Polishing scratches which are clearly visible on most of the topography pictures. They indicate that roughness profile of each film repeats the roughness profile of the substrate and does not increase. For all the experiments, double-side polished optical high-quality FS substrates were used.

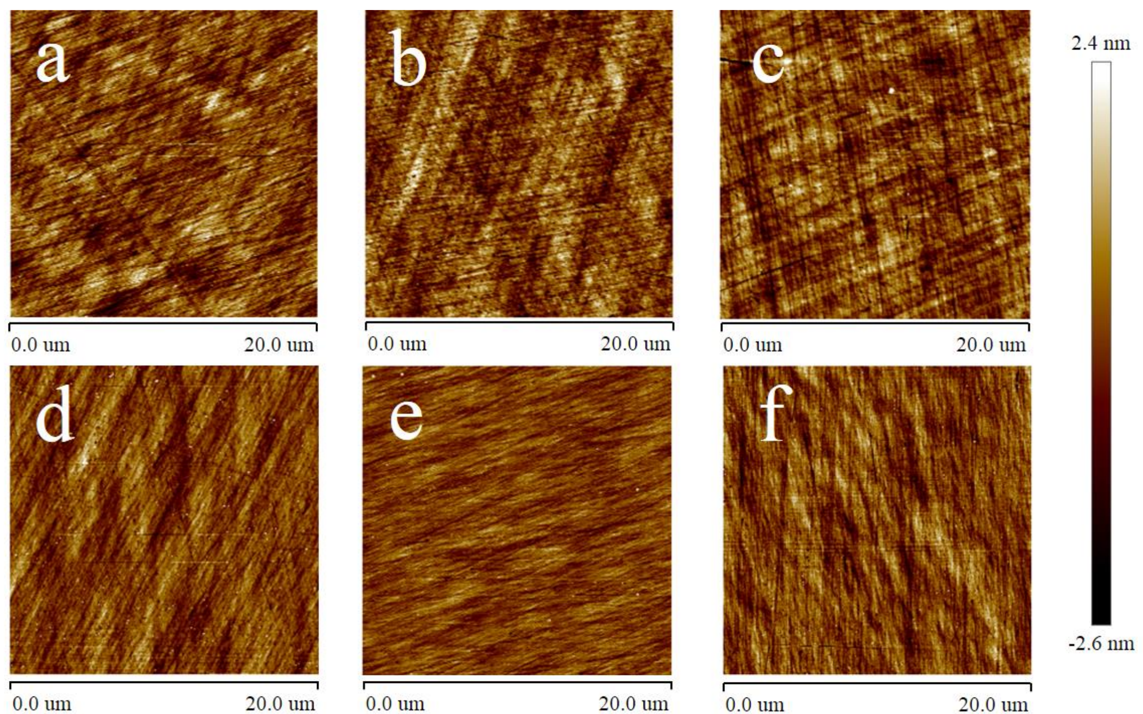

Fig. 17. Surface topography pictures of aluminum oxynitride films with various nitrogen fraction (N fraction in the film: a – 0%, b – 15%, c – 37%, d – 45%, e – 70%, f – 100%). The scale of scan is 20x20 um, color bar on the right indicates the height.

Surface roughness values were calculated from the data acquired by AFM measurements. The roughness dependence on the nitrogen fraction in the films is introduced in Fig. 18. Despite the fact that roughness values are lower for the samples with a nitrogen content over 45%, correlation between surface roughness and nitrogen content in the film is not conclusive. This discrepancy may be explained by different initial roughness of substrates which may be in the range from 0.3 to 0.5 nm. However, obtained result denotes that all produced films (from AlN to Al_2O_3, including all aluminum oxynitrides) are suitable for low roughness, high quality optical coatings production.

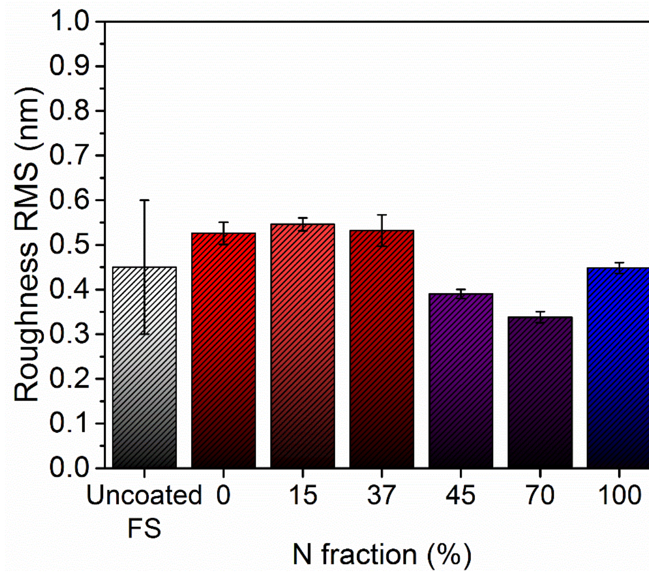

Fig. 18. Surface roughness values of aluminum oxynitride films with various nitrogen fraction.

4.3 Antireflective coatings design

In this part, coating designs for the desired specification (Table 1) were introduced and compared modelling results for aluminum nitride - aluminum oxide (*HL*) and aluminum oxynitrides materials combinations.

Table 1. The AR coatings desired specification. The values of desired reflectance, *R*, and polarization are given.

Wavelength	Single surface reflectance	Polarization
532 nm	$R < 0.5$ %	Unpolarized
1064 nm	$R < 0.5$ %	Unpolarized

In Fig. 19 the solution of the desired specification (Table 1) by using the combination aluminum nitride - aluminum oxide (*HL*) layers is introduced. Aluminum nitride was used as a high refractive index material (*H*) and aluminum oxide as low refractive index material (*L*). Similar combination for AR coating using of silicon oxide-nitride was used in Ref. [74]. Spectra (Fig. 19a) are modelled for substrate without second surface reflection. The total thickness of 4-layer *HL* coating is 290 nm: all oxide layers are 160 nm; all nitride layers are 130 nm.

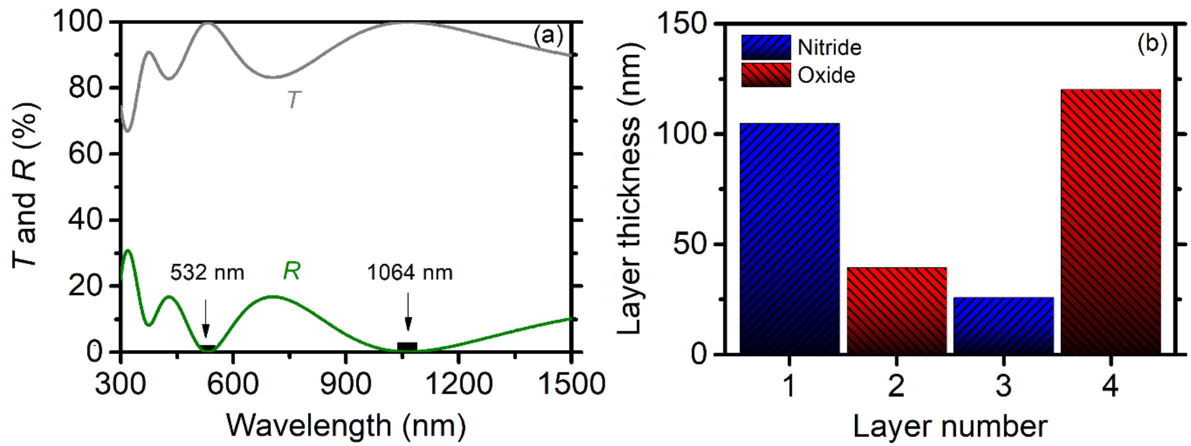

Fig. 19. Transmittance, *T*, reflectance, *R* spectra (a) and coating design (b) for optimized aluminum oxide - aluminum nitride (*HL*) antireflective coating. Total thickness of 290 nm. Desired spectral values (Table 1) are marked.

In Fig. 20 introduced the solution of the desired specification (Table 1) by using the aluminum oxynitrides layers combination. Shown spectra (Fig. 20a) are modelled for substrate without second surface reflection. The total thickness of this 3-layer oxynitrides coating is 288 nm. This coating starts with higher refractive index layer with 100% nitrogen fraction in the film and then in further layers nitrogen fraction decreased to 45 % and 15 %.

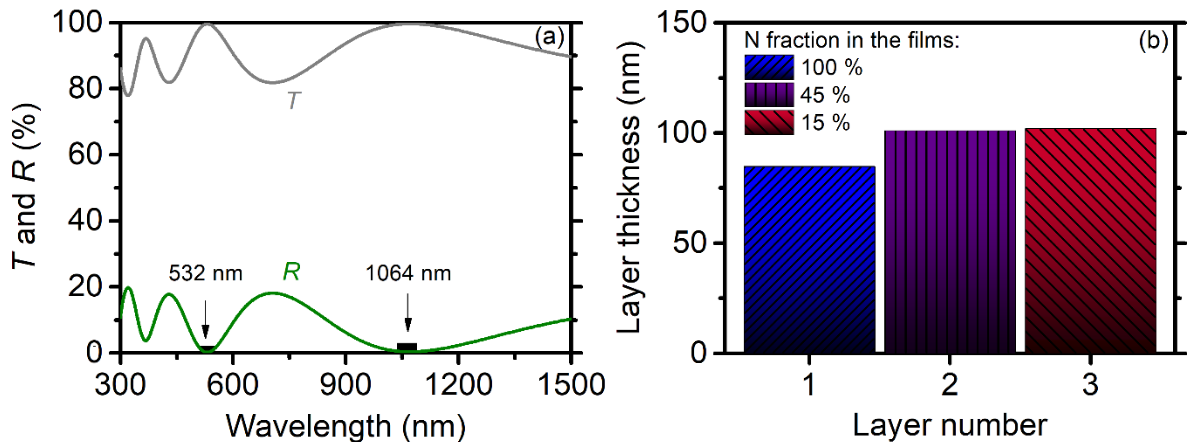

Fig. 20. Transmittance, *T*, reflectance, *R* spectra (a) and coating design (b) for optimized aluminum oxynitride with various compositions antireflective coating. Total thickness of 288 nm. Desired spectral values (Table 1) are marked.

In the case of aluminum oxynitride coating with various compositions, coating with gradient change of refractive index is reached. The comparison of refractive-index distribution is given in Fig. 21.

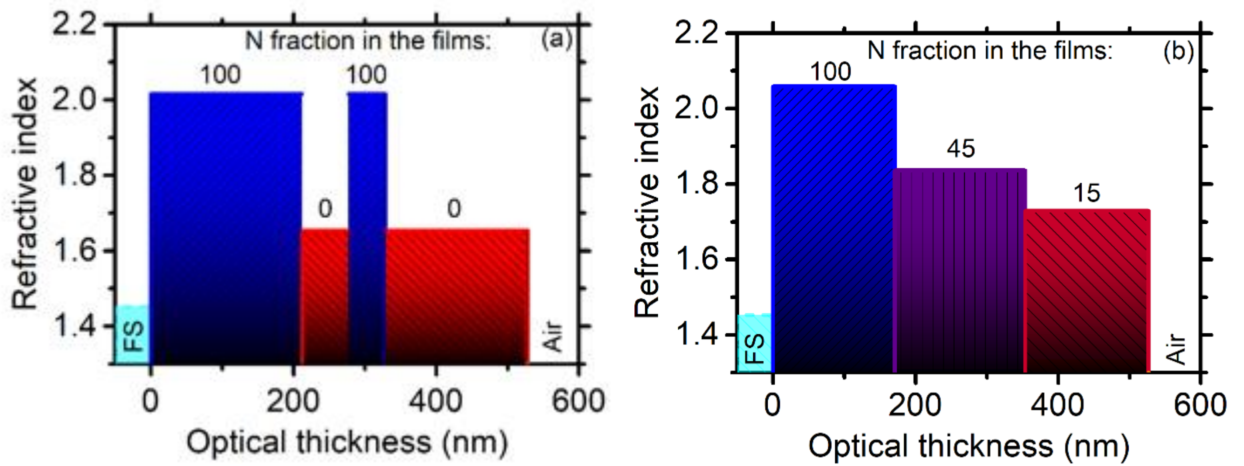

Fig. 21. Refractive-index distribution for (a) aluminum oxide - aluminum nitride (*HL*) and (b) aluminum oxynitride with various compositions antireflective coatings.

4.4 Antireflective coatings characterization

Two types of proposed coating designs (see section 4.4) were prepared using reactive magnetron sputtering in optimized conditions (see section 4.1). Formation of classical *HL* AR coating (Fig. 19) was done in 4 deposition steps, and after each layer substrates were closed by shutter. Before each layer, sputtering target was pre-sputtered and after optimized conditions (Fig. 13d) were reached. Oxynitrides AR coating preparation was done in two ways. First, it was done as classical *HL* AR coating with closing the shutter after each layer. Second, all layers were done in one continuous deposition process. In this case, after each layer gas composition was changing without closing the shutter. The gas changes between oxynitrides layers is not as significant as in *HL* case, therefore the process remained stable. Shortening of the deposition time and process steps minimizing are critical for the industry.

The *T* and *R* spectra of deposited two coating designs (Figs. 19, 20) are introduced in Fig. 22. It is seen that both coatings are within the desired specification values (Table 1). Spectral limits caused by the second surface reflection of FS substrate are also shown in Fig. 22.

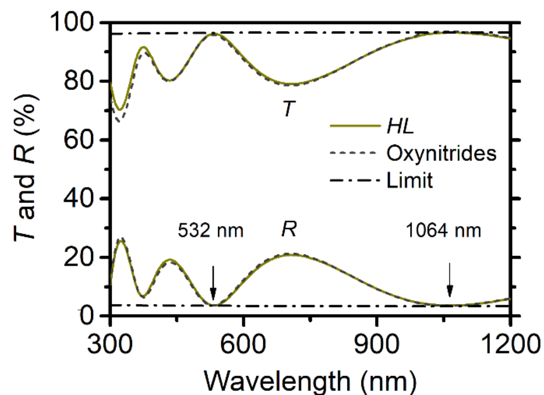

Fig. 22. Transmittance, *T,* and reflectance, *R,* spectra of AR coating made by design using HL and oxynitrides. Theoretical spectral limits for a bare fused silica substrate with the second side reflection are also shown.

The AFM measurements (Fig. 23) showed that both AR coatings have low roughness values. The root mean square roughness was lower than 0.5 nm. Low roughness values are important to avoid undesired surface scattering.

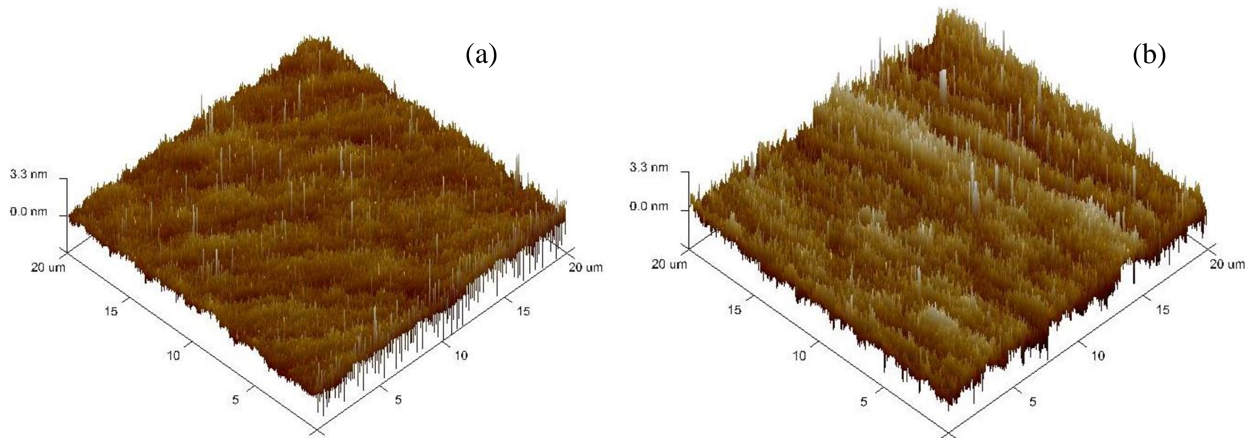

Fig. 23. AFM images of 20 × 20 μm scan area of AR coatings surface using HL (panel a) and oxynitrides (panel b).

Interferometric measurements were performed for prepared AR coatings in order to investigate flatness and stresses of the samples. High flatness and low stresses coatings are critical for high performance optical components in order to perform low distortion of the beam. Topographic views of the classical HL (a) and oxynitride (b) antireflective coatings designs are presented in Fig. 24. As it is seen from the figures, both samples are concave which indicates that coatings exhibit tensile stresses.

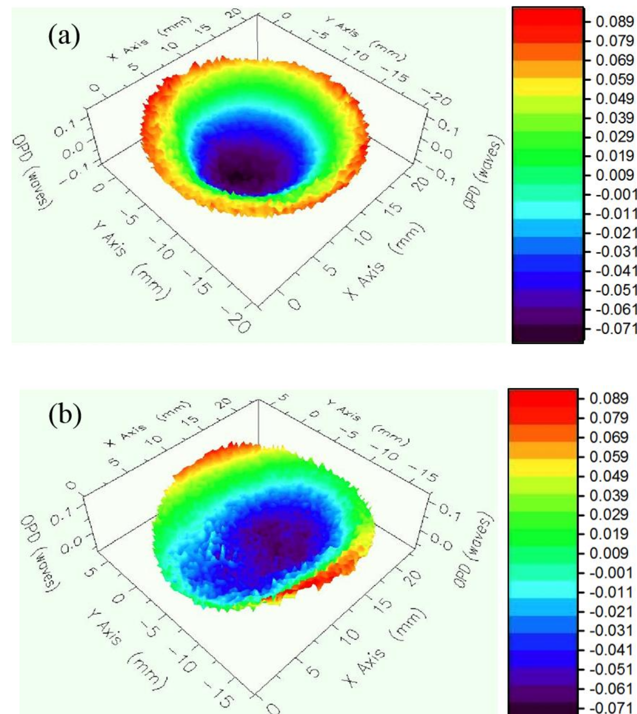

Fig. 24. Topographic view of HL (a) and oxynitrides (b) antireflective coatings acquired by interferometric flatness measurements. Wavelength used for analysis λ = 632.8 nm.

Data obtained from the interferometric flatness measurements were used for calculation of AR coatings stresses using Stoney‘s formula (Eq. 21). Calculated tensile stresses values of HL and oxynitrides design antireflective coatings are shown in Fig. 25. It illustrates that induced stress inside classical HL design sample is about 40% higher than in oxynitrides antireflective coating which is proposed in this work. This may be caused by the lower refractive indices contrast at the interface between separate layers which leads to decreased residual stresses in the coating. It is reported that the residual stresses in mixture thin films are often lower compared to the stress values of their compound components [32]. For this reason, coating with a gradual change of refractive index exhibit lower residual stress value [75]. Acquired result suggests that design consisting of gradual change of aluminum oxynitride films is promising technology for low-stress optical coatings production.

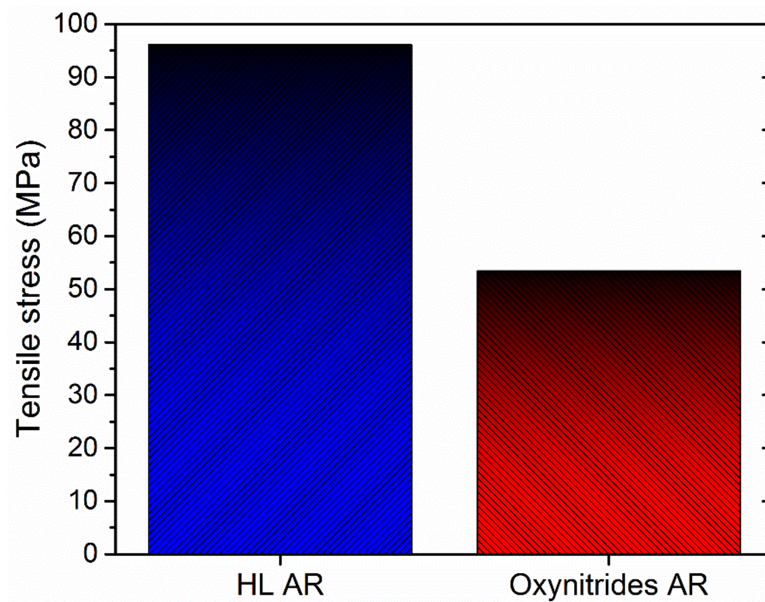

Fig. 25. Stress values comparison for HL and oxynitrides antireflective (AR) coatings.

In Fig. 26 cross-section image (TEM) of the oxynitride AR coating is introduced. It is seen that the coating is formed from 3 layers. The layer thicknesses are in agreement with the design (Fig. 20).

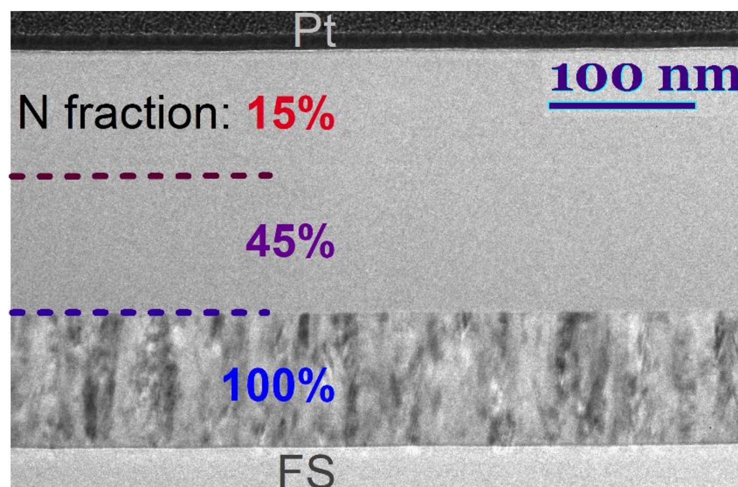

Fig. 26. Cross-section image of oxynitride AR coating.

The first layer is aluminum nitride and it is crystalline with the dense columnar structure. The second and the third are aluminum oxynitride layers and they are amorphous. Similar results for aluminum oxynitrides with various compositions were observed in Refs. [76]–[78]. Moreover, it was reported that the nitrogen-rich aluminum oxynitride films exhibit formation of hexagonal (wurtzite) AlN crystals, with a possible small amount of O atoms in their lattice. Also it occurs the preferential orientation characterized by (100) planes parallel to the film surface followed by (110) planes [79].

4.5 Quasi - Rugate filter design

In this part, quasi – Rugate filter consisting of alternating fraction aluminum oxynitride films which were described in Section 4.2 is modelled. Additionally, its spectral and electrical field characteristics are compared to classical *HL* design.

In Fig. 27 the solution of the desired specifications (Table 2) by using the combination of alternating aluminum nitride, aluminum oxide and aluminum oxynitride layers is introduced. Spectra (Fig. 27a) are modelled for substrate without second surface reflection. It is seen that modelled spectral transmittance and reflectance values are satisfying desired specifications. Fig. 27b shows sinusoidal refractive index distribution throughout the quasi – Rugate filter coating. The total physical thickness of 200 layers quasi – Rugate filter coating is 3000 nm: each layer is 15 nm of thick.

Table 2. Quasi – Rugate filter coating desired specification. The values of desired reflectance, *R*, and polarization are given.

Wavelengths	Single surface reflectance	Polarization
400 – 480 nm	$R < 12.5$ %	Unpolarized
528 - 536 nm	$T > 90$ %	Unpolarized
585 - 650 nm	$R < 12.5$ %	Unpolarized

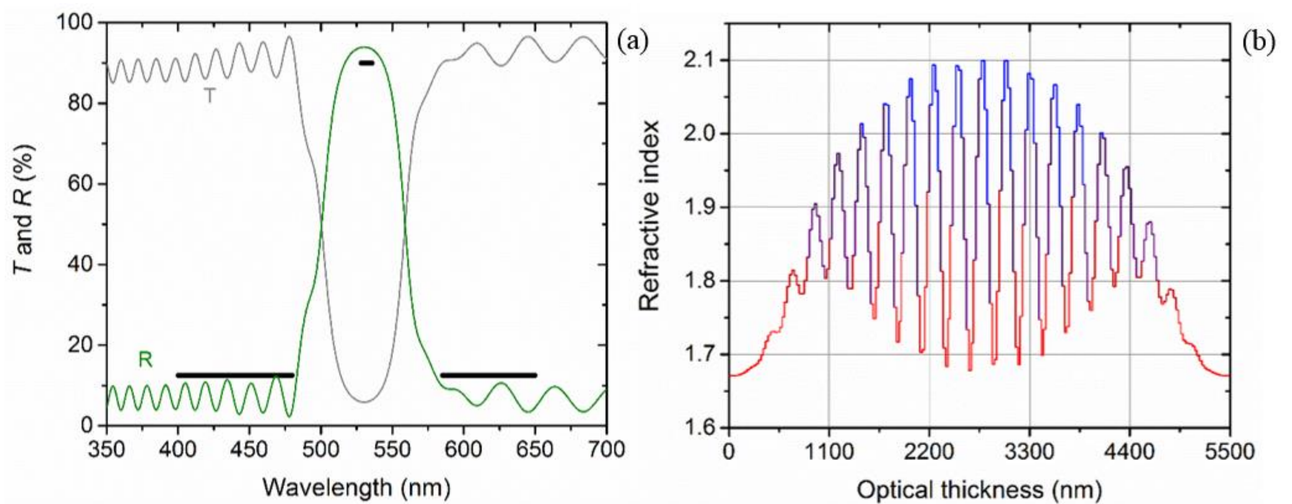

Fig. 27. Transmittance, *T*, reflectance, *R* spectra (a) and refractive index (λ = 532 nm) distribution (b) for optimized quasi – Rugate filter coating. Total physical thickness of 3000 nm. Desired spectral values (Table 2) are marked.

In Fig. 28 the modelled solution of the desired specification (Table 2) by using the combination aluminum nitride - aluminum oxide (*HL*) layers is introduced. Aluminum nitride was used as a high refractive index material (*H*) and aluminum oxide as low refractive index material (*L*). Spectra (Fig. 28a) are modelled for substrate without second surface reflection. As it is seen from spectra, high transmission zones (400 – 480 nm and 585 – 650 nm) contain ordinary sidebands of Bragg mirrors and desired reflectance values are not reached. These sidebands are influenced by high-order Fourier components of a rectangular oscillation (Fig. 28b) which might be avoided by using sinusoidal oscillation distribution of the refractive index. The total physical thickness of modelled *HL* coating (16 layers) is 1144 nm: all oxide layers are 636 nm, all nitride layers are 508 nm.

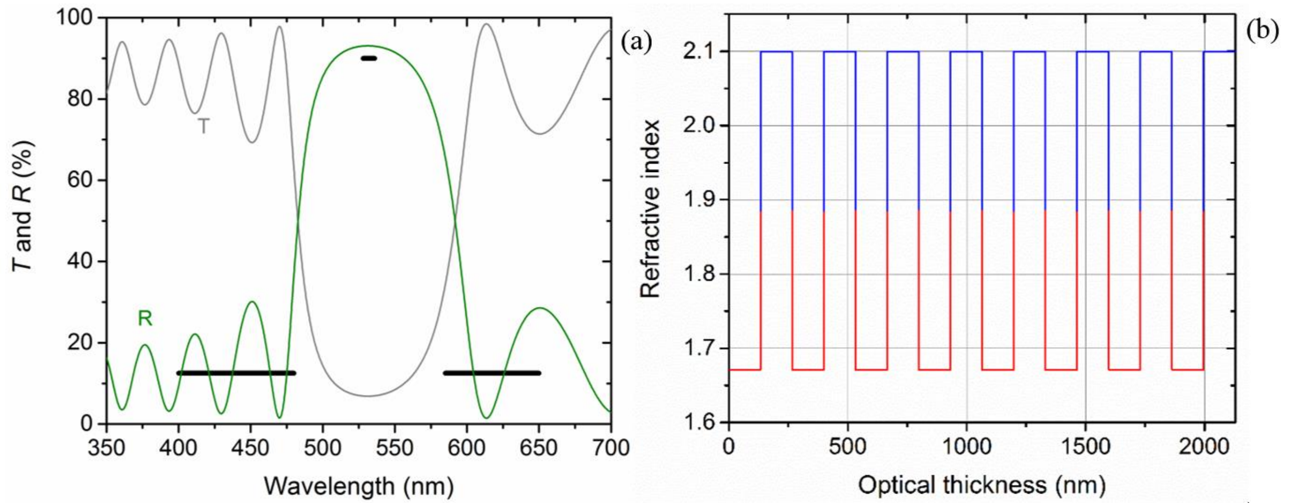

Fig. 28. Transmittance, *T*, reflectance, *R* spectra (a) and refractive index (λ = 532 nm) distribution (b) for optimized aluminum nitride - aluminum oxide (*HL*) filter coating. Total physical thickness of 1144 nm. Desired spectral values (Table 2) are marked.

It should be noted that modelled design of quasi - Rugate coating is nearly three times thicker than classical *HL* design (3000 nm to 1144 nm of physical thickness). Due to the lower contrast level of refractive indices between alternating layers in quasi – Rugate filter, thicker coating is needed in order to reach the same reflectance value as in classical *HL* design.

Electric field distribution inside the coating is one of the most important characteristics which influences laser-induced damage threshold (LIDT) of the component. Electric field and refractive indices field distributions for classical *HL* and quasi – Rugate filters designs which were introduced previously are presented in Fig. 29. It is seen that electric field intensity in the outer layers for quasi – Rugate filter is noticeably higher than in *HL* design, nevertheless it should be noted that highest peaks in quasi – Rugate design are placed in the part of the lowest refractive index oscillation. On the contrary, the very first electrical field intensity maximum is placed in inside high refractive index material (AlN) in the case of *HL* design. Moreover, electric field intensity peaks in quasi – Rugate design are placed at the parts of refractive index sinusoidal minima points, whereas in *HL* type design electric field reaches its maximum in high refractive index materials.

Having exceptionally low refractive index layers in outer side of the coating and electric field intensity maxima being positioned inside low refractive index layers throughout the coating is essentially important contributes to enhanced LIDT values in femtosecond regime of quasi – Rugate filters compared to classical *HL* stacks [80]. Moreover, it was reported that it is possible to reach up to 50% higher LIDT values than those of *HL* stacks in nanosecond regime [81]. It may be explained by the absence of the vulnerable interfaces between high refractive and low refractive index materials layers which have distinguished thermal-mechanical properties and are affected by thermal-stress induced fractures during nanosecond pulse irradiation [82].

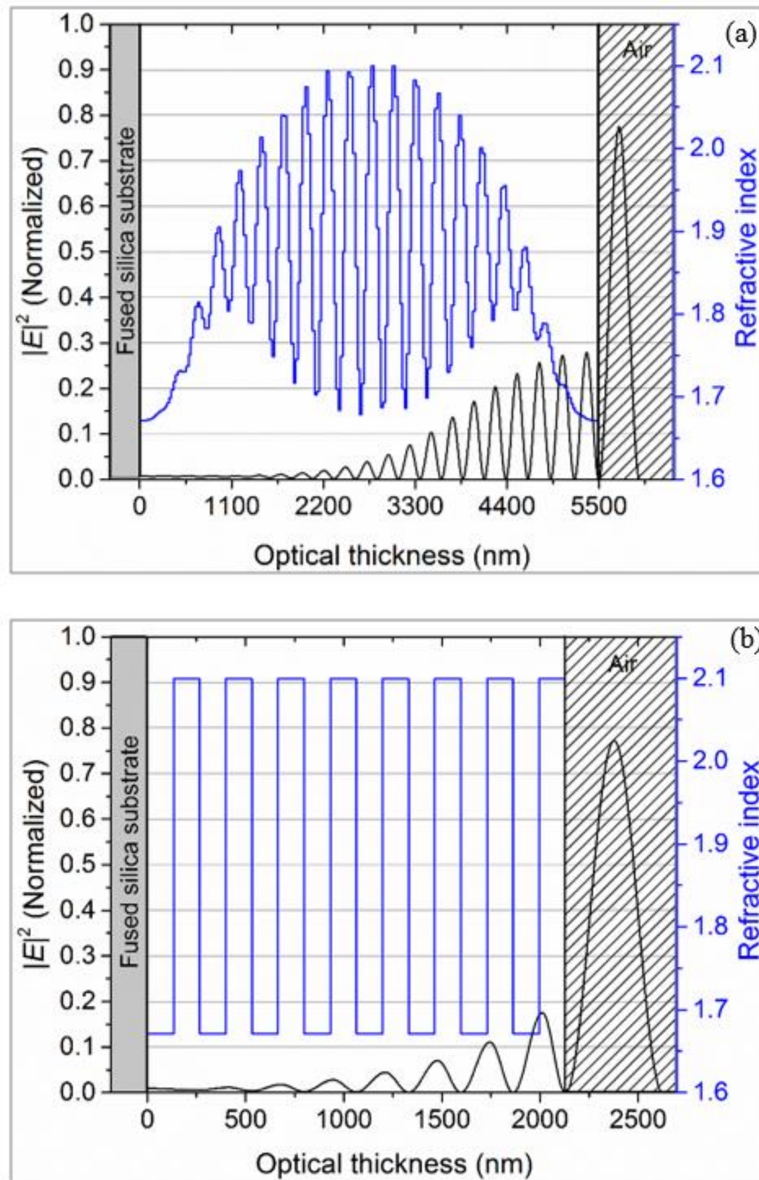

Fig. 29. Refractive index (λ = 532 nm) and electric field distribution of quasi – Rugate filter (a) and *HL* (b) filter for wavelength λ = 532 nm.

MAIN RESULTS AND CONCLUSIONS

1. It is possible to tune refractive index of deposited aluminum oxynitride mixture film while maintaining low extinction coefficient values at visible and infrared wavelengths by varying oxygen and nitrogen reactive gases flows during magnetron sputtering process while at the same time maintaining low surface roughness.
2. By using aluminum oxynitrides films it is possible to produce antireflective coatings in a smaller number of layers if compared to conventional high and low refractive index materials design and they exhibit lower stress values.
3. Numerical model of aluminum oxynitride quasi – Rugate design distinguishes itself from classical high and low refractive index materials stack design not only by its spectral characteristics but also by its electric field distribution which might lead to enhanced laser-induced damage threshold value of the coating.
4. It is shown that magnetron sputtering technology is suitable technology for effective manufacturing of aluminum oxynitrides films and multilayer coatings from one metallic target and two reactive gases.

REFERENCES

[1] H. Tsai and D. B. Bogy, "Characterization of diamondlike carbon films and their application as overcoats on thin-film media for magnetic recording", *J. Vac. Sci. Technol. A Vacuum, Surfaces, Film.*, vol. 5, no. 6, pp. 3287–3312, Nov. 1987, doi: 10.1116/1.574188.

[2] K. T. Butler, C. H. Hendon, and A. Walsh, "Designing porous electronic thin-film devices: band offsets and heteroepitaxy", *Faraday Discuss.*, vol. 201, pp. 207–219, Sep. 2017, doi: 10.1039/C7FD00019G.

[3] L. Lai, J. Wang, H. Wang, and M. Bao, "Structures and Properties of C-Doped NiCr Thin Film Deposited by Closed-Field Unbalanced Magnetron Sputtering", *J. Electron. Mater.*, vol. 46, no. 1, pp. 552–562, Jan. 2017, doi: 10.1007/s11664-016-4928-0.

[4] R. Haubner, M. Lessiak, R. Pitonak, A. Köpf, and R. Weissenbacher, "Evolution of conventional hard coatings for its use on cutting tools", *Int. J. Refract. Met. Hard Mater.*, vol. 62, pp. 210–218, Jan. 2017, doi: 10.1016/j.ijrmhm.2016.05.009.

[5] P. Spinelli, B. K. Newman, and A. Polman, "Photovoltaics: Light-Trapping in Crystalline Silicon and Thin-Film Solar Cells by Nanostructured Optical Coatings", in *Nanotechnology for Energy Sustainability*, Weinheim, Germany: Wiley-VCH Verlag GmbH & Co. KGaA, 2017, pp. 163–180.

[6] G. bong Cho *et al.*, "Facile fabrication of patterned Si film electrodes containing trench-structured Cu current collectors for thin-film batteries", *Electrochim. Acta*, vol. 224, pp. 649–659, Jan. 2017, doi: 10.1016/j.electacta.2016.12.067.

[7] J. Q. Xi *et al.*, "Optical thin-film materials with low refractive index for broadband elimination of Fresnel reflection", *Nat. Photonics*, vol. 1, no. 3, pp. 176–179, Mar. 2007, doi: 10.1038/nphoton.2007.26.

[8] E. S. Field, J. C. Bellum, and D. E. Kletecka, "Laser damage comparisons of broad-bandwidth, high-reflection optical coatings containing TiO2 , Nb2O5 , or Ta2O5 high index layers", in *Laser-Induced Damage in Optical Materials: 2013*, Nov. 2013, vol. 8885, p. 88851X, doi: 10.1117/12.2030068.

[9] V. Zhupanov, I. Kozlov, V. Fedoseev, P. Konotopov, M. Trubetskov, and A. Tikhonravov, "Production of Brewster angle thin film polarizers using a ZrO2/SiO2 pair of materials", *Appl. Opt.*, vol. 56, no. 4, p. C30, Feb. 2017, doi: 10.1364/ao.56.000c30.

[10] R. Franchy, "Growth of thin, crystalline oxide, nitride and oxynitride films on metal and metal alloy surfaces", *Surface Science Reports*, vol. 38, no. 6. Elsevier Science Publishers B.V., pp. 195–294, Jun. 01, 2000, doi: 10.1016/S0167-5729(99)00013-8.

[11] A. G. Erlat *et al.*, "Characterisation of aluminium oxynitride gas barrier films", *Thin Solid Films*, vol. 388, no. 1–2, pp. 78–86, Jun. 2001, doi: 10.1016/S0040-6090(01)00836-7.

[12] S. H. Mohamed, A. Anders, I. Montero, and L. Galán, "Structural and optical evaluation of WOxNy films deposited by reactive magnetron sputtering", *J. Phys. Chem. Solids*, vol. 68, no. 12, pp. 2227–2232, Dec. 2007, doi: 10.1016/j.jpcs.2007.06.005.

[13] B. Hallam, B. Tjahjono, and S. Wenham, "Effect of PECVD silicon oxynitride film composition on the surface passivation of silicon wafers", *Sol. Energy Mater. Sol. Cells*, vol. 96, no. 1, pp. 173–179, Jan. 2012, doi: 10.1016/j.solmat.2011.09.052.

[14] O. Banakh, P. A. Steinmann, and L. Dumitrescu-Buforn, "Optical and mechanical properties of tantalum oxynitride thin films deposited by reactive magnetron sputtering", *Thin Solid Films*, vol. 513, no. 1–2, pp. 136–141, Aug. 2006, doi: 10.1016/j.tsf.2006.01.060.

[15] R. Mientus, R. Grötschel, and K. Ellmer, "Optical and electronic properties of CrOxNy

films, deposited by reactive DC magnetron sputtering in Ar/N2/O2(N2O) atmospheres", *Surf. Coatings Technol.*, vol. 200, no. 1-4 SPEC. ISS., pp. 341–345, Oct. 2005, doi: 10.1016/j.surfcoat.2005.02.181.

[16] M. Futsuhara, K. Yoshioka, and O. Takai, "Optical properties of zinc oxynitride thin films", *Thin Solid Films*, vol. 317, no. 1–2, pp. 322–325, Apr. 1998, doi: 10.1016/S0040-6090(97)00646-9.

[17] M. Fenker, H. Kappl, O. Banakh, N. Martin, and J. F. Pierson, "Investigation of Niobium oxynitride thin films deposited by reactive magnetron sputtering", *Surf. Coatings Technol.*, vol. 201, no. 7 SPEC. ISS., pp. 4152–4157, Dec. 2006, doi: 10.1016/j.surfcoat.2006.08.104.

[18] S. Venkataraj, D. Severin, S. H. Mohamed, J. Ngaruiya, O. Kappertz, and M. Wuttig, "Towards understanding the superior properties of transition metal oxynitrides prepared by reactive DC magnetron sputtering", in *Thin Solid Films*, Apr. 2006, vol. 502, no. 1–2, pp. 228–234, doi: 10.1016/j.tsf.2005.07.280.

[19] K. Sarakinos *et al.*, "On the phase formation of sputtered hafnium oxide and oxynitride films", *J. Appl. Phys.*, vol. 108, no. 1, p. 014904, Jul. 2010, doi: 10.1063/1.3437646.

[20] S. H. Mohamed *et al.*, "Influence of nitrogen content on properties of direct current sputtered TiOxNy films", *Phys. status solidi*, vol. 201, no. 1, pp. 90–102, Jan. 2004, doi: 10.1002/pssa.200306707.

[21] B. G. Segda, M. Jacquet, and J. P. Besse, "Elaboration, characterization and dielectric properties study of amorphous alumina thin films deposited by r.f. magnetron sputtering", *Vacuum*, vol. 62, no. 1, pp. 27–38, May 2001, doi: 10.1016/S0042-207X(01)00114-2.

[22] A. Belosludtsev, N. Kyžas, A. Selskis, and R. Narbutiene, "Design, preparation and characterization of antireflective coatings using oxynitride films", *Opt. Mater.*, vol. 98, p. 109430, Dec. 2019, doi: 10.1016/j.optmat.2019.109430.

[23] N. Kyžas and A. Belosludtsev, "Investigation of Reactive Magnetron Sputtering of Aluminium Oxynitride Films and Their Applications for Optical Coatings", in *Advanced Materials and Technologies*, 2019.

[24] K. Juškevičius, "Plonųjų dielektrinių sluoksnių optinių ir fizinių savybių tyrimas bei jų formavimo technologijų optimizavimas", Vilnius University, 2014.

[25] A. Anders, "Tutorial: Reactive high power impulse magnetron sputtering (R-HiPIMS)", *J. Appl. Phys.*, vol. 121, no. 17, p. 171101, May 2017, doi: 10.1063/1.4978350.

[26] S. Swann, "Magnetron sputtering", *Phys. Technol.*, vol. 19, no. 2, p. 67, 1988, doi: 10.1088/0305-4624/19/2/304.

[27] S. Schiller, K. Goedicke, J. Reschke, V. Kirchhoff, S. Schneider, and F. Milde, "Pulsed magnetron sputter technology", *Surf. Coatings Technol.*, vol. 61, no. 1–3, pp. 331–337, Dec. 1993, doi: 10.1016/0257-8972(93)90248-M.

[28] J. Musil, P. Baroch, J. Vlček, K. H. Nam, and J. G. Han, "Reactive magnetron sputtering of thin films: Present status and trends", *Thin Solid Films*, vol. 475, no. 1-2 SPEC. ISS., pp. 208–218, 2005, doi: 10.1016/j.tsf.2004.07.041.

[29] K. Sarakinos, J. Alami, and S. Konstantinidis, "High power pulsed magnetron sputtering: A review on scientific and engineering state of the art", *Surf. Coatings Technol.*, vol. 204, no. 11, pp. 1661–1684, Feb. 2010, doi: 10.1016/j.surfcoat.2009.11.013.

[30] N. Britun, S. Konstantinidis, A. Belosludtsev, T. Silva, and R. Snyders, "Quantification of the hysteresis and related phenomena in reactive HiPIMS discharges", *J. Appl. Phys.*, vol. 121, no. 17, p. 171905, May 2017, doi: 10.1063/1.4977819.

[31] D. Depla and S. Mahieu, *Reactive Sputter Deposition, Springer Series in Materials Science, vol. 109*. Springer, 2008.

[32] K. Juškevičius *et al.*, "Fabrication of Nb2O5/SiO2 mixed oxides by reactive magnetron co-sputtering", *Thin Solid Films*, vol. 589, pp. 95–104, Aug. 2015, doi: 10.1016/j.tsf.2015.04.075.

[33] S. Schiller, G. Beister, and W. Sieber, "Reactive high rate D.C. sputtering: Deposition rate, stoichiometry and features of TiOx and TiNx films with respect to the target mode", *Thin Solid Films*, vol. 111, no. 3, pp. 259–268, Jan. 1984, doi: 10.1016/0040-6090(84)90147-0.

[34] S. Maniv, C. Miner, and W. D. Westwood, "High rate deposition of transparent conducting films by modified reactive planar magnetron sputtering of Cd2Sn alloy", in *Journal of vacuum science & technology*, Mar. 1980, vol. 18, no. 2, pp. 195–198, doi: 10.1116/1.570722.

[35] J. F. Smith, A. J. Aronson, D. Chen, and W. H. Class, "Reactive magnetron deposition of transparent conductive films", *Thin Solid Films*, vol. 72, no. 3, pp. 469–474, Oct. 1980, doi: 10.1016/0040-6090(80)90533-7.

[36] J. Vlček *et al.*, "High-rate reactive high-power impulse magnetron sputtering of hard and optically transparent HfO2 films", *Surf. Coatings Technol.*, vol. 290, pp. 58–64, Mar. 2016, doi: 10.1016/j.surfcoat.2015.08.024.

[37] P. Drude, "Zur Elektronentheorie der Metalle", *Ann. Phys.*, vol. 306, no. 3, pp. 566–613, 1900, doi: 10.1002/andp.19003060312.

[38] https://www.layertec.de/en/capabilities/coatings/metallic (accessed 2020-05-05).

[39] A. F. J. Levi and A. F. J. Levi, "The Lorentz oscillator model", in *Essential Classical Mechanics for Device Physics*, IOP Publishing, 2016.

[40] P. W. Baumeister, *Optical Coating Technology*. SPIE, 2004.

[41] H. K. Raut, V. A. Ganesh, A. S. Nair, and S. Ramakrishna, "Anti-reflective coatings: A critical, in-depth review", *Energy Environ. Sci.*, vol. 4, no. 10, pp. 3779–3804, Oct. 2011, doi: 10.1039/c1ee01297e.

[42] S. Lim, S. Shih, and J. F. Wager, "Design and fabrication of a double bandstop rugate filter grown by plasma-enhanced chemical vapor deposition", *Thin Solid Films*, vol. 277, no. 1–2, pp. 144–146, May 1996, doi: 10.1016/0040-6090(95)08002-3.

[43] W. H. Southwell and R. L. Hall, "Rugate filter sidelobe suppression using quintic and rugated quintic matching layers", *Appl. Opt.*, vol. 28, no. 14, p. 2949, Jul. 1989, doi: 10.1364/AO.28.002949.

[44] W. H. Southwell, "Gradient-index antireflection coatings", *Opt. Lett.*, vol. 8, no. 11, p. 584, Nov. 1983, doi: 10.1364/OL.8.000584.

[45] J. M. Richling, *Scratching the Surface - An Introduction to Photonics - Part 1 Optics, Thin Films, Lasers and Crystals*. 2017.

[46] H. Bartzsch, S. Lange, P. Frach, and K. Goedicke, "Graded refractive index layer systems for antireflective coatings and rugate filters deposited by reactive pulse magnetron sputtering", *Surf. Coatings Technol.*, vol. 180–181, pp. 616–620, Mar. 2004, doi: 10.1016/j.surfcoat.2003.10.105.

[47] R.-J. Xie and H. T. Bert Hintzen, "Optical Properties of (Oxy)Nitride Materials: A Review", *J. Am. Ceram. Soc.*, vol. 96, no. 3, pp. 665–687, Mar. 2013, doi: 10.1111/jace.12197.

[48] M. Serényi, M. Rácz, and T. Lohner, "Refractive index of sputtered silicon oxynitride layers for antireflection coating", *Vacuum*, vol. 61, no. 2–4, pp. 245–249, May 2001, doi:

10.1016/S0042-207X(01)00124-5.

[49] S. Lange, H. Bartzsch, P. Frach, and K. Goedicke, "Pulse magnetron sputtering in a reactive gas mixture of variable composition to manufacture multilayer and gradient optical coatings", *Thin Solid Films*, vol. 502, no. 1–2, pp. 29–33, Apr. 2006, doi: 10.1016/j.tsf.2005.07.229.

[50] S. Venkataraj, O. Kappertz, R. Jayavel, and M. Wuttig, "Growth and characterization of zirconium oxynitride films prepared by reactive direct current magnetron sputtering", *J. Appl. Phys.*, vol. 92, no. 5, pp. 2461–2466, Sep. 2002, doi: 10.1063/1.1498963.

[51] R. Ruppin, "Validity Range of the Maxwell-Garnett Theory", *Phys. Status Solidi*, vol. 87, no. 2, pp. 619–624, Jun. 1978, doi: 10.1002/pssb.2220870227.

[52] D. Stroud, "The effective medium approximations: Some recent developments", *Superlattices Microstruct.*, vol. 23, no. 3–4, pp. 567–573, Mar. 1998, doi: 10.1006/spmi.1997.0524.

[53] K. Oughstun and N. Cartwright, "On the Lorentz-Lorenz formula and the Lorentz model of dielectric dispersion", *Opt. Express*, vol. 11, no. 13, p. 1541, Jun. 2003, doi: 10.1364/oe.11.001541.

[54] S. Muthukumaran *et al.*, "The optimisation of ultrasonic cleaning procedures for dairy fouled ultrafiltration membranes", in *Ultrasonics Sonochemistry*, Jan. 2005, vol. 12, no. 1-2 SPEC. ISS., pp. 29–35, doi: 10.1016/j.ultsonch.2004.05.007.

[55] V. Janicki, J. Sancho-Parramon, S. Yulin, M. Flemming, and A. Chuvilin, "Optical and structural properties of Nb 2O 5-SiO 2 mixtures in thin films", *Surf. Coatings Technol.*, vol. 206, no. 17, pp. 3650–3657, Apr. 2012, doi: 10.1016/j.surfcoat.2012.03.015.

[56] R. M. Phelan, "PSEUDO-DERIVATIVE-FEEDBACK (PDF) CONTROL.", Livermore, CA (United States), Jan. 1971. doi: 10.2172/4711540.

[57] A. V. Tikhonravov, M. K. Trubetskov, and T. V. Amotchkina, "Optical monitoring strategies for optical coating manufacturing", in *Optical Thin Films and Coatings: From Materials to Applications*, Elsevier, 2018, pp. 65–101.

[58] "Optilayer software". [Online]. Available: http://www.optilayer.com/ (accessed 2020-05-05).

[59] S. A. Furman and A. Tikhonravov, *Basics of optics of multilayer systems*, Frontieres. Gif-sur-Yvette, 1992.

[60] N. Jalili, K. L.- Mechatronics, and undefined 2004, "A review of atomic force microscopy imaging systems: application to molecular metrology and biological sciences", *Elsevier*, Accessed: May 24, 2020.

[61] G. C. A. M. Janssen, M. M. Abdalla, F. van Keulen, B. R. Pujada, and B. van Venrooy, "Celebrating the 100th anniversary of the Stoney equation for film stress: Developments from polycrystalline steel strips to single crystal silicon wafers", *Thin Solid Films*, vol. 517, no. 6, pp. 1858–1867, Jan. 2009, doi: 10.1016/j.tsf.2008.07.014.

[62] https://www.slideshare.net/HARSHALVARADE/interferometry (accessed 2020-05-05).

[63] https://cmrf.research.uiowa.edu/transmission-electron-microscopy (accessed 2020-05-05).

[64] O. Fursenko *et al.*, "Optical properties and band gap characterization of high dielectric constant oxides", *Thin Solid Films*, vol. 520, no. 14, pp. 4532–4535, May 2012, doi: 10.1016/j.tsf.2011.10.195.

[65] A. Belosludtsev *et al.*, "Correlation between stoichiometry and properties of scandium oxide films prepared by reactive magnetron sputtering", *Appl. Surf. Sci.*, vol. 427, pp. 312–318,

Jan. 2018, doi: 10.1016/j.apsusc.2017.08.068.

[66] F. Vaz, N. Martin, and M. Fenker, *Metallic oxynitride thin films by reactive sputtering and related deposition methods: Processes, properties and applications*. 2013.

[67] J. R. Rumble, D. R. Lide, and T. J. Bruno, *CRC handbook of chemistry and physics : a ready-reference book of chemical and physical data.* .

[68] C. Rousselot and N. Martin, "Influence of two reactive gases on the instabilities of the reactive sputtering process", *Surf. Coatings Technol.*, vol. 142–144, pp. 206–210, Jul. 2001, doi: 10.1016/S0257-8972(01)01195-1.

[69] A. Belosludtsev *et al.*, "Structure and properties of Hf-O-N films prepared by high-rate reactive HiPIMS with smoothly controlled composition", *Ceram. Int.*, vol. 43, no. 7, 2017, doi: 10.1016/j.ceramint.2017.01.102.

[70] S. Dreer, R. Krismer, P. Wilhartitz, and G. Friedbacher, "Statistical evaluation of refractive index, growth rate, hardness and Young's modulus of aluminium oxynitride films", *Thin Solid Films*, vol. 354, no. 1–2, pp. 43–49, 1999.

[71] K. S. Shamala, L. C. S. Murthy, and K. Narasimha Rao, "Studies on optical and dielectric properties of Al2O3 thin films prepared by electron beam evaporation and spray pyrolysis method", *Mater. Sci. Eng. B*, vol. 106, no. 3, pp. 269–274, Feb. 2004, doi: 10.1016/j.mseb.2003.09.036.

[72] E. O. Filatova and A. S. Konashuk, "Interpretation of the Changing the Band Gap of Al2O3 Depending on Its Crystalline Form: Connection with Different Local Symmetries", *J. Phys. Chem. C*, vol. 119, no. 35, pp. 20755–20761, Sep. 2015, doi: 10.1021/acs.jpcc.5b06843.

[73] S. Cho, "Effect of nitrogen flow ratio on the structural and optical properties of aluminum nitride thin films", *J. Cryst. Growth*, vol. 326, no. 1, pp. 179–182, Jul. 2011, doi: 10.1016/j.jcrysgro.2011.01.092.

[74] T.-J. Gim, B.-J. Lee, and P.-K. Shina, "Anti-reflection Coating Application of Si x O y-Si x N y Stacked-Layer Fabricated by Reactive Sputtering", *J. Korean Vac. Soc.*, vol. 19, no. 5, pp. 341–346, 2010.

[75] C.-J. Tang, C.-C. Jaing, K.-S. Lee, and C.-C. Lee, "Residual stress in Ta2O5-SiO2 composite thin-film rugate filters prepared by radio frequency ion-beam sputtering", *Appl. Opt.*, vol. 47, no. 13, p. C167, May 2008, doi: 10.1364/AO.47.00C167.

[76] J. Musil, R. Jílek, M. Meissner, T. Tölg, and R. Čerstvý, "Two-phase single layer Al-O-N nanocomposite films with enhanced resistance to cracking", *Surf. Coatings Technol.*, vol. 206, no. 19–20, pp. 4230–4234, May 2012, doi: 10.1016/j.surfcoat.2012.04.028.

[77] J. Borges, N. Martin, F. Vaz, and L. Marques, "Process monitoring during AlN x O y deposition by reactive magnetron sputtering and correlation with the film's properties", *J. Vac. Sci. Technol. A Vacuum, Surfaces, Film.*, vol. 32, no. 2, p. 021307, Mar. 2014, doi: 10.1116/1.4863957.

[78] K. Jiang, K. Sarakinos, S. Konstantinidis, and J. M. Schneider, "Low temperature synthesis of α-Al2O3 films by high-power plasma-assisted chemical vapour deposition", *J. Phys. D. Appl. Phys.*, vol. 43, no. 32, p. 325202, Aug. 2010, doi: 10.1088/0022-3727/43/32/325202.

[79] A. Belosludtsev, J. Vlček, J. Houška, S. Haviar, and R. Čerstvý, "Tunable composition and properties of Al-O-N films prepared by reactive deep oscillation magnetron sputtering", *Surf. Coatings Technol.*, vol. 392, p. 125716, Jun. 2020, doi: 10.1016/j.surfcoat.2020.125716.

[80] M. Jupé, M. Lappschies, L. Jensen, K. Starke, and D. Ristau, "Improvement in laser irradiation resistance of fs- dielectric optics using silica mixtures", Oct. 2006, p. 64031A,

doi: 10.1117/12.696131.

[81] Y. Pu *et al.*, "Enhanced thermomechanical stability on laser-induced damage by functionally graded layers in quasi-rugate filters", *Appl. Surf. Sci.*, vol. 440, pp. 288–293, May 2018, doi: 10.1016/j.apsusc.2018.01.138.

[82] Z. Qiao, P. Ma, H. Liu, Y. Pu, and Z. Liu, "Laser-induced damage of rugate and quarter-wave stacks high reflectors deposited by ion-beam sputtering", *Opt. Eng.*, vol. 52, no. 8, p. 086103, Aug. 2013, doi: 10.1117/1.OE.52.8.086103.

SUMMARY

Formation of Aluminum Oxynitride Thin Films and Their Application for Optical Coatings

Naglis Kyžas

The aim of this work is to investigate possible applications of aluminum oxynitride thin films in optical coatings. In order to reach the aim, several tasks must be done: 1) investigate reactive magnetron sputtering process with metallic aluminum target and two reactive gases; 2) characterize deposited aluminum oxynitride films with various nitride fractions; 3) model and characterize multilayer antireflective coating using aluminum oxynitride layers; 4) model quasi – Rugate filter consisting of alternating fraction aluminum oxynitride films.

Investigation of reactive sputtering modes while changing reactive gases composition (oxygen and/or nitrogen) was done. It was determined that with the increase of nitrogen content in reactive gas, the moment of target poisoning is shifting to the higher flow values. Also high-rate, stable process optimized reactive gases flows were found.

Samples with various nitrogen fraction in the films were prepared. Their refractive indices and extinction coefficients were modelled. It was shown that by varying oxygen and nitrogen flows as reactive gases during magnetron sputtering process it is possible to tune refractive index of deposited thin film from pure Al_2O_3 to pure AlN. Surface roughness and band gap values of the films were evaluated.

Antireflective coatings with conventional high and low refractive index layers structure and aluminum oxynitride films gradual refractive index change structure were compared. It was shown that both coatings satisfy desired spectral specifications and maintain low roughness values of the coating. However, it was found that antireflective coatings using oxynitride thin films exhibit two times smaller coating stress than conventional high and low refractive index layers structure.

Comparison of conventional high and low refractive index layers and quasi – Rugate filters showed that quasi – Rugate filter design enables opportunity to reach better spectral characteristics in high transmittance zone. Moreover, investigation of electric field distribution in the coatings suggests that quasi – Rugate filter should perform higher laser – induced damage threshold values than typical high and low refractive index layers coating.

SANTRAUKA

Aliuminio oksinitrido plonų sluoksnių formavimas ir jų taikymas optinėse dangose

Naglis Kyžas

Šio darbo tikslas yra ištirti galimus aliuminio oksinitrido plonų sluoksnių taikymus optinėse dangose. Tikslui pasiekti, išsikeltos šios užduotys: 1) ištirti reaktyvųjį magnetroninio dulkinimo procesą, dulkinant metalinį taikinį dviejų reaktyviųjų dujų atmosferoje; 2) charakterizuoti nusodintus aliuminio oksinitrido sluoksnius su skirtinga nitrido frakcija. 3) suprojektuoti ir charakterizuoti daugiasluoksnę skaidrinančią dangą, naudojant aliuminio oksinitrido sluoksnius. 4) suprojektuoti kvazi *Rugate* tipo filtrą, naudojant kintamos aliuminio oksinitrido frakcijos sluoksnius.

Atliktas reaktyviojo dulkinimo režimų, keičiant reaktyviųjų dujų sudėtį (deguonis ir/ar azotas), tyrimas. Nustatyta, kad didėjant azoto kiekiui reaktyviųjų dujų sudėtyje, taikinio užsiteršimo momentas slenka link aukštesnių srauto verčių. Taip pat rastos didelės spartos, stabilaus ir optimizuoto proceso reaktyviųjų dujų srautų vertės.

Paruošti bandiniai su skirtingomis nitridų koncentracijomis (0 %; 15 %; 37 %; 45 %; 70 % ir 100 %) sluoksniuose. Nustatyta, kad sluoksnių lūžio rodikliai didėja didėjant nitrido daliai sluoksniuose. Ekstinkcijos koeficiento vertės, didėjant nitrido frakcijai, padidėjo nežymiai ir visiems sluoksniams išliko $k_{532} < 1x10^{-4}$. Tokiu būdu, keičiant deguonies ir azoto kaip reaktyviųjų dujų srautus magnetroninio dulkinimo proceso metu, galima reguliuoti nusodinamo sluoksnio lūžio rodiklį nuo $n_{532}(Al_2O_3)=1.67$ iki $n_{532}(AlN)=2.1$. Apskaičiuotos nusodintų sluoksnių draustinių energijų juostos tarpo vertės. Didžiausiu draustinių juostos tarpu pasižymi Al_2O_3 sluoksnis (E_g = 5.85 eV), tuo tarpu mažiausiu – AlN (E_g = 3.87 eV). Likusių sluoksnių draustinių energijų juostos tarpų vertės yra tarp šių reikšmių ir stebima atvirkštinė priklausomybė tarp draustinio energijų juostos tarpo ir nitrido koncentracijos sluoksnyje verčių. Taip pat atlikti šių bandinių paviršiaus šiurkštumo matavimai atominių jėgų mikroskopu. Gautos vertės parodo, kad bandinių šiurkštumas, kintant nitrido koncentracijai sluoksniuose, nekinta, todėl šiuos sluoksnius galima naudoti aukštos kokybės optinių dangų gamybai.

Sumodeliuoti, palyginti ir charakterizuoti siekiamų charakteristikų ($R < 0.5$ % ties bangos ilgiais 532 nm ir 1064 nm) dangų dizainai iš aliuminio nitrido – aliuminio oksido (*HL*) ir aliuminio oksinitrido medžiagų kombinacijų. Pademonstruota, kad oksinitrido sluoksniai leidžia pagaminti skaidrinančias dangas susidedančias iš mažiau sluoksnių nei įprastame aukšto ir žemo lūžio rodiklio medžiagų dizaine.Abiejų magnetroninio dulkinimo metodu pagamintų skaidrinančių dangų spektrinės charakteristikos tenkina siektinas. Atlikti abiejų skaidrinančių dangų plokštiškumo matavimai parodė, kad abi dangos pasižymi tempiamaisiais įtempiais. Dangų įtempių verčių analizė parodė, kad

skaidrinančios oksinitridinės dangos įtempiai yra apie 2 kartus mažesni nei *HL* dizaino skaidrinančios dangos. Paviršiaus šiurkštumo matavimai parodė, kad abiem atvejais yra išlaikomos žemos dangų šiurkštumo vertės.

Sumodeliuotos įprastinė aukšto ir mažo lūžio rodiklių, naudojant AlN ir Al_2O_3 sluoksnius, ir kvazi *Rugate* tipo, naudojant kintamo lūžio rodiklio aliuminio oksinitrido sluoksnius, spektrinių filtrų ties λ = 532 nm dangos. Kvazi *Rugate* filtro atveju yra išvengiama spektrinių osciliacijų aukšto pralaidumo zonoje, kurios atsiranda esant standartiniam *Brego* tipo veidrodžiui. Elektrinio lauko pasiskirstymo tyrimas šiuose dviejų dangų tipuose parodė, kad išoriniuose dangos sluoksniuose kvazi *Rugate* filtro atveju elektrinis laukas yra didesnis nei aukšto ir žemo lūžio rodiklio dangos atveju, tačiau išoriniuose šios dangos filtro sluoksniuose yra mažiausio lūžio rodiklio medžiagos sluoksniai, o įprastos konstrukcijos dangos atveju, intensyvumo pikas yra pasiekiamas ties pirmuoju aukšto lūžio rodiklio medžiagos sluoksniu. Taip pat, elektrinio lauko intensyvumo pikai kvazi *Rugate* dangoje susiformuoja sinusoidinio lūžio rodiklių osciliacijų minimumuose, o įprastos žemo ir mažo lūžio rodiklių atveju, pikas pasiekiamas ties aukšto lūžio rodiklio medžiagomis. Šios savybės leidžia tikėtis gauti išaugusias lazerinės pažaidos vertes.